Reclamation of Tidal Flats Within Tidal Basins Alters Centennial Morphodynamic Adaptation to Sea-Level Rise

Guo, Leicheng; Zhu, Chunyan; Xu, Fan; Xie, Weiming; van der Wegen, Mick; Townend, Ian; Wang, Zheng Bing; He, Qing

DOI
10.1029/2021JF006556

Publication date
2022

Document Version
Final published version

Published in
Journal of Geophysical Research: Earth Surface

Citation (APA)
Guo, L., Zhu, C., Xu, F., Xie, W., van der Wegen, M., Townend, I., Wang, Z. B., & He, Q. (2022). Reclamation of Tidal Flats Within Tidal Basins Alters Centennial Morphodynamic Adaptation to Sea-Level Rise. *Journal of Geophysical Research: Earth Surface*, *127*(6), Article e2021JF006556. https://doi.org/10.1029/2021JF006556

JGR Earth Surface

RESEARCH ARTICLE
10.1029/2021JF006556

Reclamation of Tidal Flats Within Tidal Basins Alters Centennial Morphodynamic Adaptation to Sea-Level Rise

Leicheng Guo[1], Chunyan Zhu[1,2], Fan Xu[1], Weiming Xie[1], Mick van der Wegen[3,4], Ian Townend[5], Zheng Bing Wang[2,4], and Qing He[1]

[1]State Key Lab of Estuarine and Coastal Research, East China Normal University, Shanghai, China, [2]Faculty of Civil Engineering and Geosciences, Delft University of Technology, Delft, The Netherlands, [3]IHE Delft, Delft, The Netherlands, [4]Deltares, Delft, The Netherlands, [5]School of Ocean and Earth Science, University of Southampton, Southampton, UK

Abstract Reclamation of low-lying tidal flats and floodplains adjacent to present shorelines has been implemented worldwide for both coastal defense and development. While it is technically feasible to monitor the short-term impact of tidal flat embankments, it is challenging to identify long-term and cumulative morphodynamic impact, particularly considering centennial sea-level rise (SLR). In this study, we construct a process-based hydro-morphodynamic model for a schematized tidal basin and examine its morphodynamic evolution under the combined influence of SLR and tidal flat embankments. We see that rising sea levels lead to inundation of low-lying floodplains just above high water, creating new intertidal flats that mitigate the drowning impact of SLR. This mitigation effect is lost if the low-lying floodplains and tidal flats are reclaimed, preventing any shoreline migration under SLR. Removing a large portion of intertidal flats within the tidal basin induces significant changes in basin hypsometry and potentially, a reversal of flood/ebb dominance. The resulting hydro-morphodynamic impact of large-scale tidal flat embankment is more significant than SLR at a centennial time scale. This suggests a need for much greater management awareness regarding the cumulative impact of human activities. These findings imply that allowing lateral shoreline migration under SLR sustains tidal basin's inherent morphodynamic buffering capacity, whereas reclaiming tidal flats significantly alters hydro-morphodynamic adaptation at the decadal to centennial time scales. It highlights the importance of conserving low-lying floodplains and tidal flats in tide-dominated systems to counteract the drowning impact of SLR.

Plain Language Summary Tidal estuaries and deltas host valuable wetlands and ecosystems wordwidely. They are also vulnerable to sea level rise (SLR) and human intervention when tidal flats are reclaimed to generate new land and to defend coasts from erosion and flooding. Recently, nature-based solutions like wetland restoration have become increasingly popular in coastal management practice. However, the benefits of these approaches are not yet fully explored. Using a large-scale morphodynamic model of a schematized tide-dominated basin, we find that morphodynamic adaptation of an unconstrained basin under SLR mitigates the drowning effect by lateral shoreline migration, extending the tidal flats landwards. Reclamation of tidal flats, however, reduces the surface area, tidal prism and intertidal storage volumes within the tidal basin, which may even induce a regime shift from sediment export to import. SLR then exacerbates the impact of tidal flat embankments. These findings suggest that tidal flat losses can fundamentally change tidal systems' hydro-morphodynamic adaptation at decadal to centennial time scales, and confirm the importance of conserving and restoring tidal wetlands.

Key Points:

- Progressive tidal inundation of low-lying land adjacent to existing tidal flats enables them to migrate landwards in response to sea level rise (SLR)
- Whether this maintains, extends or reduces the area of tidal flat, depends on the topography adjacent to the tidal basin
- Large-scale reclamation of intertidal areas can have a more significant impact on morphology than SLR at the centennial time scale

Supporting Information:

Supporting Information may be found in the online version of this article.

Correspondence to:

L. Guo,
lcguo@sklec.ecnu.edu.cn

Citation:

Guo, L., Zhu, C., Xu, F., Xie, W., van der Wegen, M., Townend, I., et al. (2022). Reclamation of tidal flats within tidal basins alters centennial morphodynamic adaptation to sea-level rise. *Journal of Geophysical Research: Earth Surface*, *127*, e2021JF006556. https://doi.org/10.1029/2021JF006556

Received 20 DEC 2021
Accepted 14 JUN 2022

1. Introduction

Coastal wetlands provide important habitats that host valuable ecosystems. Currently they are facing increasing pressure from climate change and sea-level rise (SLR). The global SLR has risen by 0.2 ± 0.05 m between 1901 and 2018, with a rate of 3.7 ± 0.5 mm yr^{-1} in the 2006–2018 periods (IPCC, 2021). SLR is likely to accelerate in the coming century, adding another 0.28–1.01 m till 2100 (Chen et al., 2017; IPCC, 2021). A worldwide concern is that accretion of coastal tidal flats (mainly the intertidal zones) and salt marshes may not be able to keep pace with an accelerating SLR rate (Best et al., 2018; Zhang et al., 2020), resulting in coastal erosion and shoreline retreat, drowning of salt marshes and habitats, and increased flood risk (Craft et al., 2009; Kirwan & Megonigal, 2013; Lovelock et al., 2015; Valiela et al., 2018). Land subsidence and a decline in river-borne sediment supply may further exacerbate coastal erosion and wetland losses (Syvitski et al., 2009).

A number of studies has examined hydrodynamic impact of SLR on tidal basins (tide-dominated semi-enclosed bodies) and estuaries (Du et al., 2018; Friedrichs et al., 1990; Rodriguez et al., 2017; Talke & Jay, 2020) and hydro-morphodynamic impact on tidal inlets, estuaries and deltas (Best et al., 2018; Dissanayake et al., 2012; Elmilady et al., 2019; Leuven et al., 2019; van de Lageweg and Slangen, 2017; van der Wegen, 2013; van Maanen et al., 2013). The majority of these studies suggest that the accretion rates of intertidal flats cannot meet the accelerating rates of SLR and are likely to drown (Elmilady et al., 2019; Leuven et al., 2019; van der Wegen, 2013; van Maanen et al., 2013). In some exceptional cases like the Waddenzee tidal flats may survive from low, linear SLR scenarios, depending on sediment import rates (Wang et al., 2018). As a result, it is expected that 40%–90% of global coastal wetlands will be lost due to SLR by the end of the 21st century (Ganju et al., 2017; Spencer et al., 2016; Valiela et al., 2018).

These studies have typically assumed that a fixed shoreline position. In the contexts of marine transgression, this implies a stationary rather than dynamic response within the landscape. However, marine transgression provides a mechanism that can mitigate tidal wetland loss by inundation of and sedimentation over low-lying floodplains adjacent to coastal shorelines under SLR (Allen, 1990). Tidal basins and estuaries are commonly surrounded by large areas of low-lying hinterland, which is naturally just above high water and can be inundated under higher mean sea levels (Dalrymple & Choi, 2007). The global coastal wetland loss rate was estimated to be 30% in the coming century, if wetlands can migrate landward and under the assumption that there is sufficient sediment supply (Schuerch et al., 2018). The fate of a tidal basin, to be raised or drowned, then depends on its ability to accrete vertically at rates equal to or larger than SLR, and/or to migrate inland at rates faster than shoreline erosion (Townend et al., 2021).

However, intensified coastal development has resulted in profound "coastal squeeze" owing to dike and jetty constructions for the purpose of road construction, land reclamation, realigning port and waterways, and coastal defense works (Doody, 2004). Globally, while the land area at deltas has increased because of land reclamation (Nienhuis et al., 2020), the areas of deltaic intertidal flats and habitat have decreased by 16% in the period of 1984–2016 (Murray et al., 2019). Regionally, over 80% of wetlands have been lost in US in agricultural area (Zelder, 2004), while tidal flats and habitat have shrunk by 86% in Southern California since 1870 as a result of fast urbanization and coastal development (Stein et al., 2010). In China, approximately 59% of coastal saltmarshes were lost between the 1980 and 2010s due to land reclamation (Gu et al., 2018), by the intensive land reclamation in the Changjiang River and Pearl River deltas (Ma et al., 2019). "Coastal squeeze" exposes a conflict between coastal safety and ecosystem conservation and has become a significant management challenge.

The profound impact of human activities on the hydro-morphodynamics in tidal estuaries and basins has received increasing awareness and research effort (Talke & Jay, 2020). The coastal management community is increasingly aware that hard engineering protection (e.g., dikes and levees) of coastal systems may not be sustainable over the longer term (Temmerman et al., 2013). Dikes need maintenance and upgrades, and their failure under extreme storm events may cause catastrophic disasters. Dikes and embankments reduce tidal inundation, change the coastal ecosystem, and prevent landward incursion as the sea level rises. For example, Donatelli et al. (2018) reported that loss and erosion of tidal flats and saltmarshes can change the tidal hydrodynamics, resulting in reduced sediment trapping and marsh growth.

This challenge is increasingly being addressed by the adoption of the concepts like managed realignment (e.g., de-embankment, de-poldering, set back, and wetland mitigation banks) and nature-based solutions (Temmerman et al., 2013; Townend & Pethick, 2002), that is, making more room for rivers and estuaries. Numerous studies suggest that restoring coastal ecosystems and maintaining a certain width of foreland tidal flats and salt marshes can reduce stress on more inland dikes, stimulate ecosystem restoration and effectively reduce coastal flooding and erosion risk (Doody, 2004; Mazik et al., 2010; Reed et al., 2018; Schuerch et al., 2018; Temmerman et al., 2013; Townend & Pethick, 2002). Managed realignment schemes were developed in several cases around the world (e.g., the Humber Estuary, Mazik et al., 2010). Mangrove and other salt-tolerant species were planted to further reinforce the foreland of embankment. While it is technically feasible to monitor and detect the short-term impact of tidal flat losses on hydrodynamics and sediment transport, the influences of tidal flat embankment and the benefit of managed retreat to restore coastal wetlands on the long-term and large-scale morphodynamics have been insufficiently examined, particularly under the SLR conditions at the decadal to centennial time scales that is relevant to management and planning (Mariotti & Canestrelli, 2017). A proper understanding of the long-term

hydro-morphodynamic adaptation under the influence of tidal flat embankment and SLR is needed to support robust management decision making.

As an example, the surface area of the North Branch in the Changjiang Delta has approximately halved in the period of 1974–2018 (Li et al., 2020), predominantly due to extensive reclamation of tidal flats. A flood dominance and associated sediment import has established since the 1950s when river influences minimized owing to degenerated inflow conditions (Guo et al., 2021; Obodoefuna et al., 2020; see Figure S1 in Supporting Information SI). Strong sediment import then led to fast tidal flat accretion, followed by progressive tidal flat reclamation, which was hypothesized to further enhance sediment import and initiate a positive feedback (Guo et al., 2021). The long-term impact of a substantial loss of tidal flats on the branch was seemingly overlooked in previous studies, whereas such knowledge is necessary to better understand the morphological response and, hence, aid management decision making. However, field data are seldom available to verify the large-scale and long-term impact of tidal flat embankment, and it is technically difficult to isolate and quantify the possible small changes related to SLR and embankment from other factors for specific cases. To address this challenge, in this work we employ a hydro-morphodynamic model to explore the long-term impact of tidal flat embankment under varying levels of SLR. The findings from such modeling exercises would provide insights on the large-scale impact of extensive human activities, thus possibly shedding lights on management of the North Branch in the Changjiang Delta. The rest of this work is organized with Section 2 introducing the modeling methods and parameter settings, Section 3 presenting modeled hydrodynamics, sediment flux and morphology, Section 4 discussing the model implications and Section 5 setting out the main conclusions.

2. Modeling Methods

2.1. Model Setup

Instead of modeling the actual North Branch and the whole Changjiang Delta, in this work we take the North Branch as an independent tide-dominated channel and build up a schematized model to explore the large-scale impact of tidal flat embankment. This is because the Changjiang delta is an extremely large domain (700 × 100 km), which imposes a high computational demand for long-term morphodynamic simulations. In addition, strong spatial variations in physical parameter settings pose particular challenges in calibrating long-term hydro-morphodynamics, Although simplified, our schematized approach would benefit insight into the generic response and reveal some of the likely impacts of tidal flat embankment that can inform management of other tide-dominated estuaries and basins around the world.

The schematized tidal basin model was constructed based on the Delft3D software (Lesser et al., 2004). The tidal basin is 150 km long and has a prescribed convergent planform with laterally convex-up tidal flat profiles (Figure 1). It discharges into a coastal ocean with a gentle shelf slope. The model mesh has a higher resolution inside the tidal basin and around the mouth regions, with a cell size of 50 m, to resolve the channels and shoals forming therein, while the cell size increased slowly to 200 m toward to the edge of the domain where morphodynamic changes remained limited. The initial tidal channel width at the mean sea level increases from 1 km at the land end to 15 km at the mouth section, forming a funnel-shaped planform. Following van der Wegen and Roelvink (2008), the initial tidal channel has a linearly sloping bed with water depth varying from 0 m at the landward end to 15 m at the tidal channel mouth, and deepening to 50 m at the seaward boundary. The initial cross-section profile combines a U-shaped sub-tidal channel in the landward segment and convex-up inter- and supra-tidal flats in the lower segment, suggesting the initial presence of inter- and supra-tidal flats (Figure 1). The transverse inter-tidal flat slope is 1/500–1/1500 on average in the lower estuary, which is close to the mean value observed in actual estuaries (Le Hir et al., 2000). The convex-up tidal flats were chosen to be consistent with the fact that tidal flats are broadly present in highly convergent seaward regions within tidal estuaries and basins (Dalrymple & Choi, 2007) and that tide-dominated flats are more likely to develop convex-up profiles owing to the constructive tidal forcing condition (Friedrichs, 2011; Kirby, 2000).

The model is driven by tides only, mimicking a tide-dominated environment, similar to previous studies (Hibma et al., 2003; van der Wegen, 2013; van der Wegen and Roelvink, 2008; van Maanen et al., 2013). An astronomical semi-diurnal tidal constituent of 1.5 m in amplitude is imposed at the seaward boundary. For simplicity, river impact is excluded in this work to focus on the morphodynamic sensitivity to SLR and tidal flat losses, although

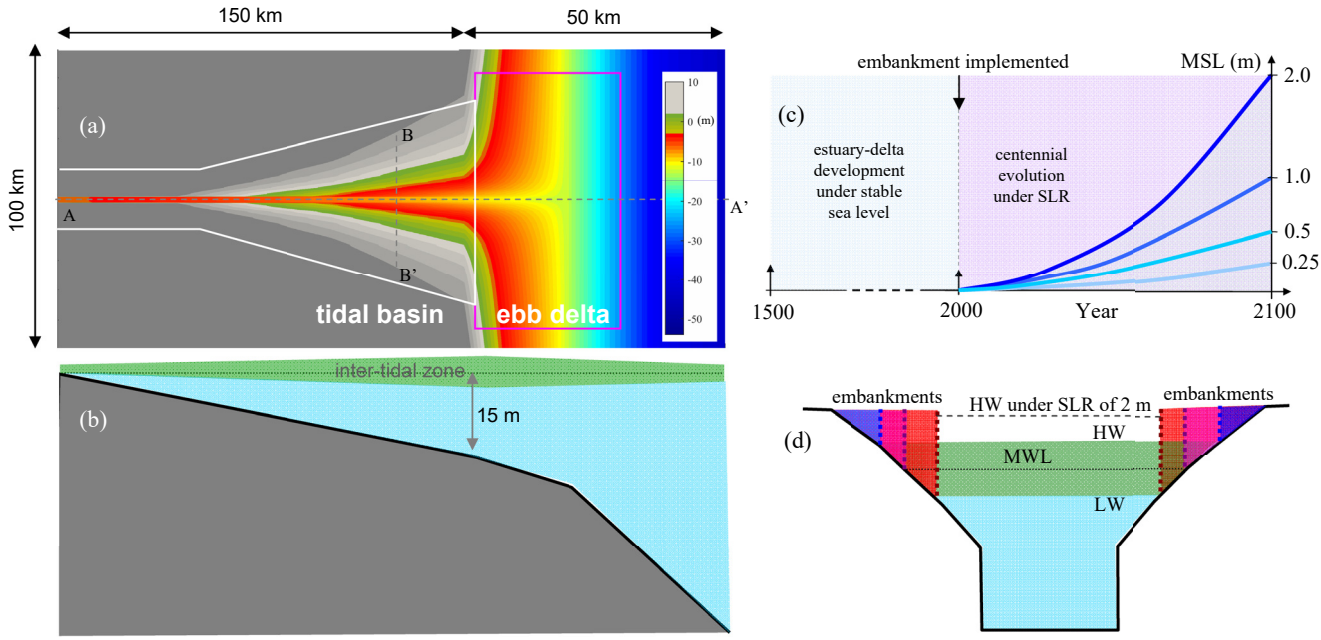

Figure 1. The geometrical setting of the schematized tidal basin: (a) plan view and (b) side view (A-A'), (c) the sea-level rise scenarios with accelerating increase rates of mean sea level, and (d) the initial cross-section profile (B-B') and the scenarios of different degree of tidal flat embankment. HW, LW, and MWL indicate high water, low water, and mean water level, respectively.

it is known that river flow is likely to play an important role in modulating hydrodynamics and sediment transport and inducing morphodynamics changes in estuaries (Guo et al., 2014; Olabarrieta et al., 2018; Zhou et al., 2020).

Transport of non-cohesive sediment with a grain size of 150 μm is simulated by the Engelund and Hansen (1967) formula. This formulation considers both suspended and bedload transport as total transport, and uses a power function of current velocity. Preliminary simulations considering other sediment grain sizes exhibit similar morphodynamic patterns but varying morphodynamic time scales, reflecting the fact that sediment transport rate is a negative function of grain size. Long-term morphodynamic development is achieved by using the morphological factor approach (Roelvink & Reniers, 2011), that is, a morphological factor of 100 after preliminary simulation tests. Dry bed erosion is enabled by prescribing erosion occurring in wet cells to the adjacent dry cells (Deltares, 2011), in order to allow for bank erosion, channel migration and erosion of emergent sand bars. Land subsidence or uplift, and the presence of vegetation have not been considered. Although simplified, the geometric size and forcing conditions of the schematized tidal basin are overall consistent with the North Branch of Changjiang Delta (Guo et al., 2021; see Figure S1 in Supporting Information SI). An idealized representation was adopted here to gain insight into the generic response of this specific class of tidal systems. The details of model setting are detailed in Table 1.

2.2. Scenario Setting

Starting from the initial bathymetry, the morphodynamic model is first run for a period (500 years in this study) during which morphodynamic evolution leads to a well-developed channel-shoal system (see the supplementary Movie S1). The morphology at the end of 500-year, which is close to a dynamic equilibrium state (but not a static equilibrium), was used as the initial bathymetry for the following 100-year sensitivity scenarios considering SLR and embankment. The scenario excluding SLR and embankment was used as a reference case. Sensitivity scenarios were defined by (a) considering exponential SLR of 0.25, 0.5, 1.0, and 2.0 m over 100 years (Figure 1c), that is, SLR rate of 2.5, 5, 10, and 20 mm yr^{-1} on average, respectively. These are approximately representative of the IPCC Representative Concentration Pathways: RCP 2.6 (small), RCP 4.5 (medium), RCP 8.5 (high), and the high-end projections (extremely high); (b) reclaiming tidal flats surrounding the main channel (but not the tidal flats attached to the sand bars in the middle of the channel) at varying degrees (Figure 1d). This was achieved by imposing thin dams positioned at the envelopes of high water, mean tidal level, and low water on the 500-year

Table 1
Model Parameter Settings Based on the Delft3D Software

Property	Parameter setting
domain size	(150 + 50) km*100 km
cell size	50–200 m
initial channel bed slope	0–15 m
width convergence	convergence length L_b of 270 km (using $B = B_o e^{-Lb/x}$)
lateral flat slope	1/500–1/1,500
bed roughness	uniform Chezy 65 $m^{1/2}/s$
tidal amplitude	1.5 m at the sea side boundary
sediment	noncohesive with grain size of 150 μm
sediment transport formula	Engelund and Hansen (1967)
initial bed sediment thickness	50 m
hydrodynamic time step	60 s
hydrodynamic run time	5 years + 1 year
morphological factor	100
morphodynamic time	500 years + 100 years
dry bed erosion parameter	1
lateral bed slope factor (alfaBn)	10

bathymetry, representing reclamation of the supra-tidal flats (low degree of embankment), high intertidal flats (medium degree of embankment), and all intertidal flats (high degree of embankment), respectively; and (c) considering both SLR and tidal flat embankment.

The different extents of tidal flat embankment imply that the initial geometry condition for the 100-year sensitivity simulations varies, as summarized in Table 2. In all cases the initial volume and planimetric area of the channel at low water are the same. In total there were 20 sensitivity simulations, which enabled straightforward comparison to reveal the impact of both SLR and embankment (Table 2). For example, the reference case NE-noSLR examines the situation with no embankment and no SLR, whereas the HE-SLR200 scenario considers a high degree of embankment (high extent of tidal flat loss) and a SLR of 2.0 m. To be clear, high embankment scenarios refer to the highest loss of intertidal area.

Model results in terms of morphological patterns, intertidal flat area and storage volume, tidally averaged sediment flux are compared to the reference case to highlight the impact of SLR and tidal flat embankment. The sediment flux at the mouth section of the tidal basin (km-150) is used to indicate the sediment import or export regime, for both the cumulated flux over the 100-year and the tidally averaged flux. Morphodynamic changes within the tidal basin (landward km-150) and over the ebb-tidal delta (seaward km-150) are discussed separately, to inform the impact of tidal flat reclamation. It is noted that the tidal basin and the ebb-tidal delta are inherently connected, for example, sediment export indicates net sediment transport from the tidal basin to the ebb-tidal delta, and vice verse.

3. Model Results

3.1. Morphodynamic Development

Starting from the prescribed initial morphology, the first 500-year morphodynamic simulation (representing the historical morphodynamic development) leads to well-developed meandering channels within the tidal basin (see the supplementary Movie S1 and Figure 4a). To the seaward of the basin, an ebb-tidal delta with bifurcated distributary channels develops because of sediment export from the tidal basin. This model-generated channel pattern matches well with the conceptual model of Dalrymple and Choi (2007). However, the meandering channel pattern within the basin is different from the North Branch, and the distributary channel structure over the ebb-tidal delta is more bifurcated. This is probably because of the excluded fine sediment transport and wave

Table 2
*Definition of the 20 Sensitivity Scenarios Considering Sea-Level Rise From 0 to 2.0 m Over 100 Years and Embankment of Varying Degrees. *CSF Indicates Cumulative Sediment Flux Over 100 Years at the Mouth Section of the Tidal Basin*

Scenario	Tidal flat loss	SLR (m)	A1 (10^9 m^3)	A2 (10^9 m^3)	CSF* (10^6 m^3)	Rising tide duration (hr)	Falling tide duration (hr)	TSF (10^4 m^3)
NE-noSLR		0		6.32	19.93	5.94	6.06	3.86
NE-SLR025		0.25		6.46	20.89	5.91	6.09	3.64
NE-SLR050	none	0.5	4.86	6.73	21.28	5.92	6.08	3.70
NE-SLR100		1.0		7.07	22.73	5.91	6.09	4.39
NE-SLR200		2.0		8.15	25.81	5.91	6.09	6.56
LE-noSLR		0		6.44	19.17	5.99	6.01	2.60
LE-SLR025		0.25		6.60	19.27	6.00	6.00	2.75
LE-SLR050	low	0.5	4.85	6.86	19.82	5.96	6.04	2.92
LE-SLR100		1.0		7.22	20.07	5.91	6.09	2.75
LE-SLR200		2.0		7.74	19.71	5.88	6.12	2.22
ME-noSLR		0		5.61	6.91	5.79	6.21	0.68
ME-SLR025		0.25		5.72	6.99	5.73	6.27	0.53
ME-SLR050	medium	0.5	4.74	5.82	6.60	5.74	6.26	0.33
ME-SLR100		1.0		5.96	5.43	5.66	6.34	-0.08
ME-SLR200		2.0		6.07	3.70	5.58	6.42	-0.75
HE-noSLR		0		4.45	-2.47	5.54	6.46	-0.53
HE-SLR025		0.25		4.49	-2.49	5.55	6.45	-0.53
HE-SLR050	high	0.5	4.42	4.53	-2.62	5.56	6.44	-0.44
HE-SLR100		1.0		4.62	-2.96	5.54	6.46	-0.58
HE-SLR200		2.0		4.78	-3.44	5.50	6.50	-0.58

Note. Tidal prism (A2), rising and falling tidal duration, and the cross-section integrated tide-averaged sediment flux (TSF) were evaluated during a single tidal cycle at the mouth section based on the morphology at the end of 100-year sensitivity simulations. Tidal prism A1 showed the value at the beginning of the 100-year simulations. Positive values of CSF and TSF indicate sediment export, and negative values indicate sediment import.

impact that can stimulate sand bar merging and reduce the number of channels (Edmonds & Slingerland, 2010). The morphology at the end of the 500-year is considered to be close to a dynamic morphodynamic equilibrium, given that a mature channel-shoal pattern had become established and the tidally averaged sediment transport flux at the mouth had slowed down (Figure S2 in Supporting Information SI).

In the subsequent 100-year simulations (representing the future evolution), the overall channel pattern persists (Figures 2a and 4b), but with strong erosion and deposition occurring due to channel and shoal migration (Figure 4f). Under SLR, the tidal basin becomes wider due to lateral shoreline expansion (Figures 3a and 4c). The ebb-tidal delta continues to prograde in the SLR scenarios, but at a smaller rate compared to the reference case. Implementing tidal flat embankment, however, reduces the bankful basin width, surface area, and tidal prism (Figures 2 and 3). The development of the ebb-tidal delta becomes slower in the embankment scenarios (Figures 4d and 5). Adding SLR in the embankment scenarios induces less apparent changes in morphology compared to the embankment only situation, suggesting more profound impact of tidal flat loss than SLR (Figures 4e and 5).

3.2. Changes in Tidal Hydrodynamics

The changes in tidal resonance are insignificant other than the slightly more amplified tidal waves under SLR and embankment scenarios. The mean water levels are less elevated and the longitudinal mean water level gradients are slightly smaller in the embankment scenarios compared with the reference case (Figure 6a). The M_2 tide is slightly more amplified in the embankment scenarios, particularly in the lower segments of the tidal basin where more tidal flats are reclaimed (seaward km-65). In the landward section of the tidal basin, a slight reduction in M_2 amplitude occurs in the medium embankment scenarios. The impact of tidal flat embankment on tidal

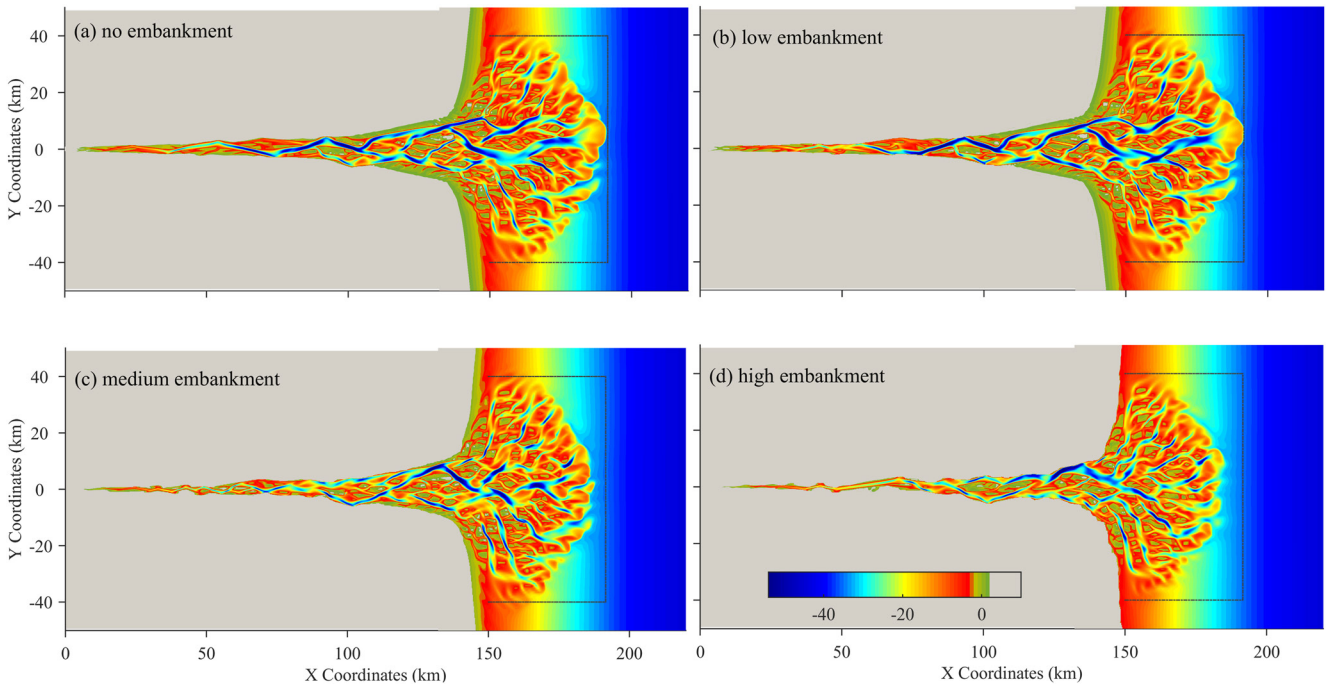

Figure 2. The morphology at the end of 100-year sensitivity simulations in the scenarios considering embankment but not sea-level rise (SLR): (a) NE-noSLR, (b) LM-noSLR, (c) ME-noSLR, and (d) HE-noSLR. The dashed lines provide a reference for the ebb-delta region.

wave propagation is comparatively more significant than that of SLR. Specifically, the M_2 tidal amplitude was 0.1–0.2 m larger in the embankment scenarios than in the SLR scenarios (Figure 6b). The local generation of M_4 overtide is less profound in the embankment scenarios, particularly in the landward regions, other than the slightly larger M_4 in the lower parts of the basin (seaward km-65) in the high embankment scenarios (Figure 6c).

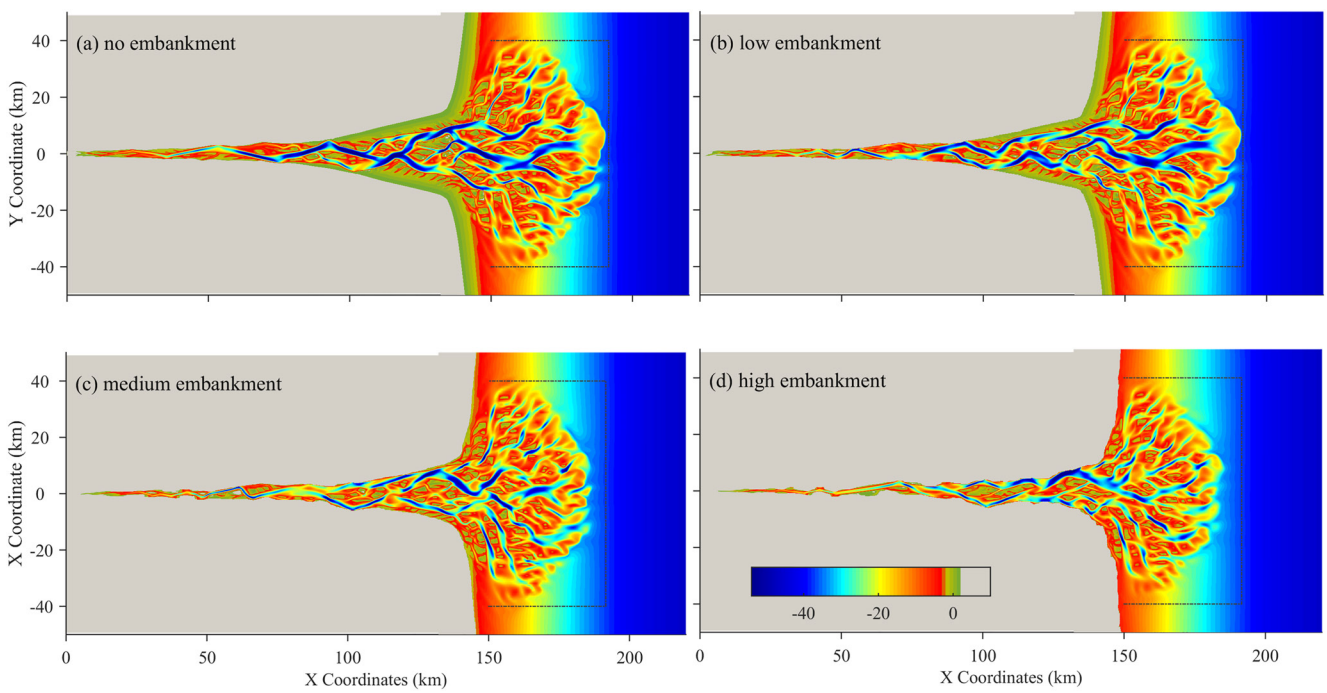

Figure 3. The morphology at the end of 100-year sensitivity simulations in the scenarios considering embankment and sea-level rise (SLR) of 2.0 m: (a) NE-SLR200, (b) LM-SLR200, (c) ME-SLR200, and (d) HE-SLR200. The dashed lines provide a reference for the ebb-delta region.

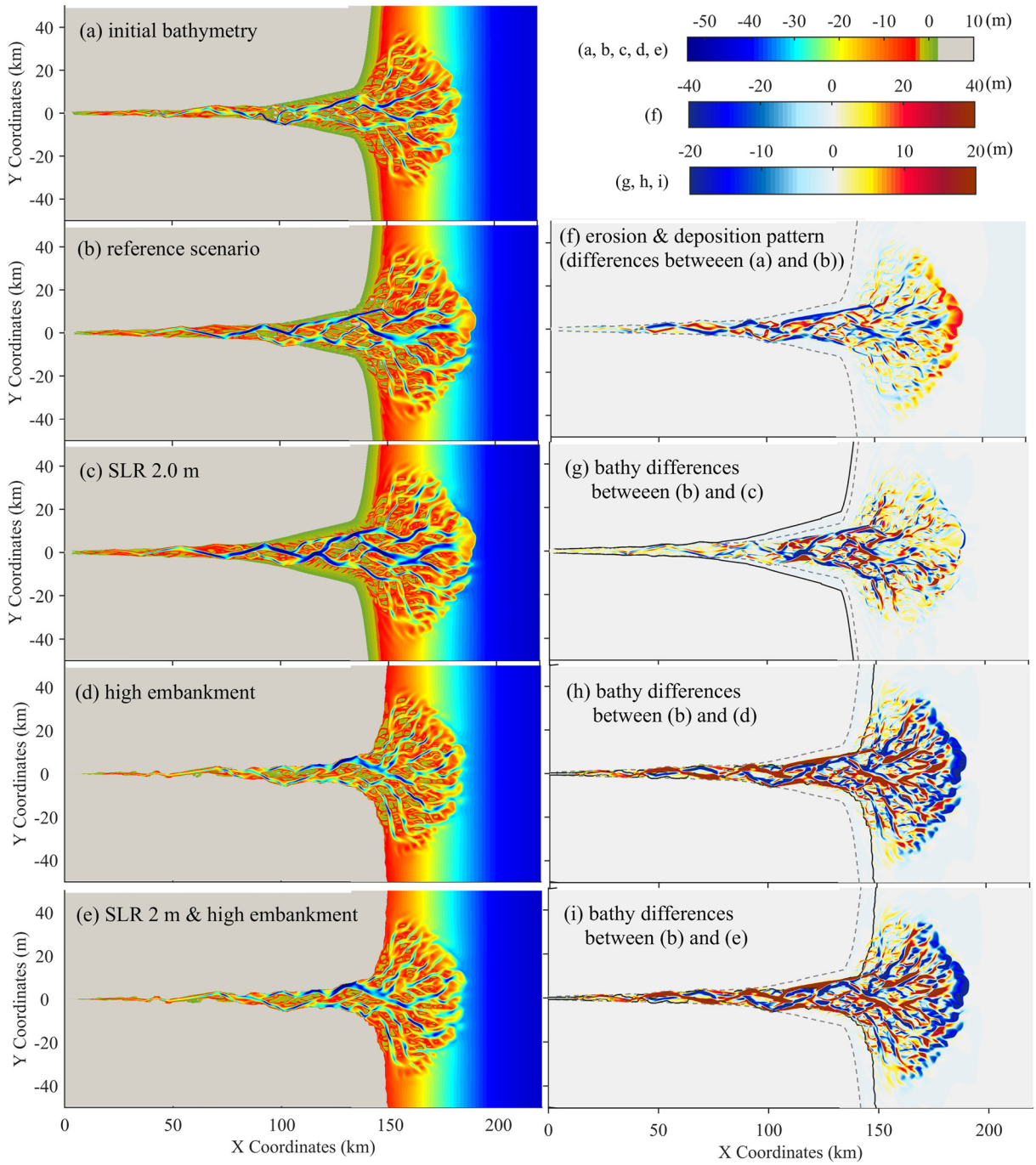

Figure 4. (a) The morphology after 500-year development (which was used as the initial bathymetry in the sensitivity simulations), and the morphology after 100-year in the (b) reference scenario (NE-noSLR), (c) sea-level rise (SLR) of 2.0 m scenario (NE-SLR200), (d) high embankment scenario (HE-noSLR), and (e) both SLR of 2.0 m and high embankment scenario (HE-SLR200), and (f) the erosion and deposition pattern of reference scenario over 100 years, and the bathymetry differences (g) between panels (b) and (c), (h) between panels (b) and (d), and (i) between panels (b) and (e). The panels (c) and (e) display the absolute water depth considering a 2 m SLR. The green shades in panels (a) to (e) roughly indicate the intertidal flats. Positive and negative values in panels (f)–(i) indicates deposition and erosion, respectively. The dashed lines in panels (f) to (i) indicate the shoreline (corresponding to high tide) in the reference scenario and the solid lines in panels (g) to (i) are new shorelines in the high SLR and high embankment scenarios.

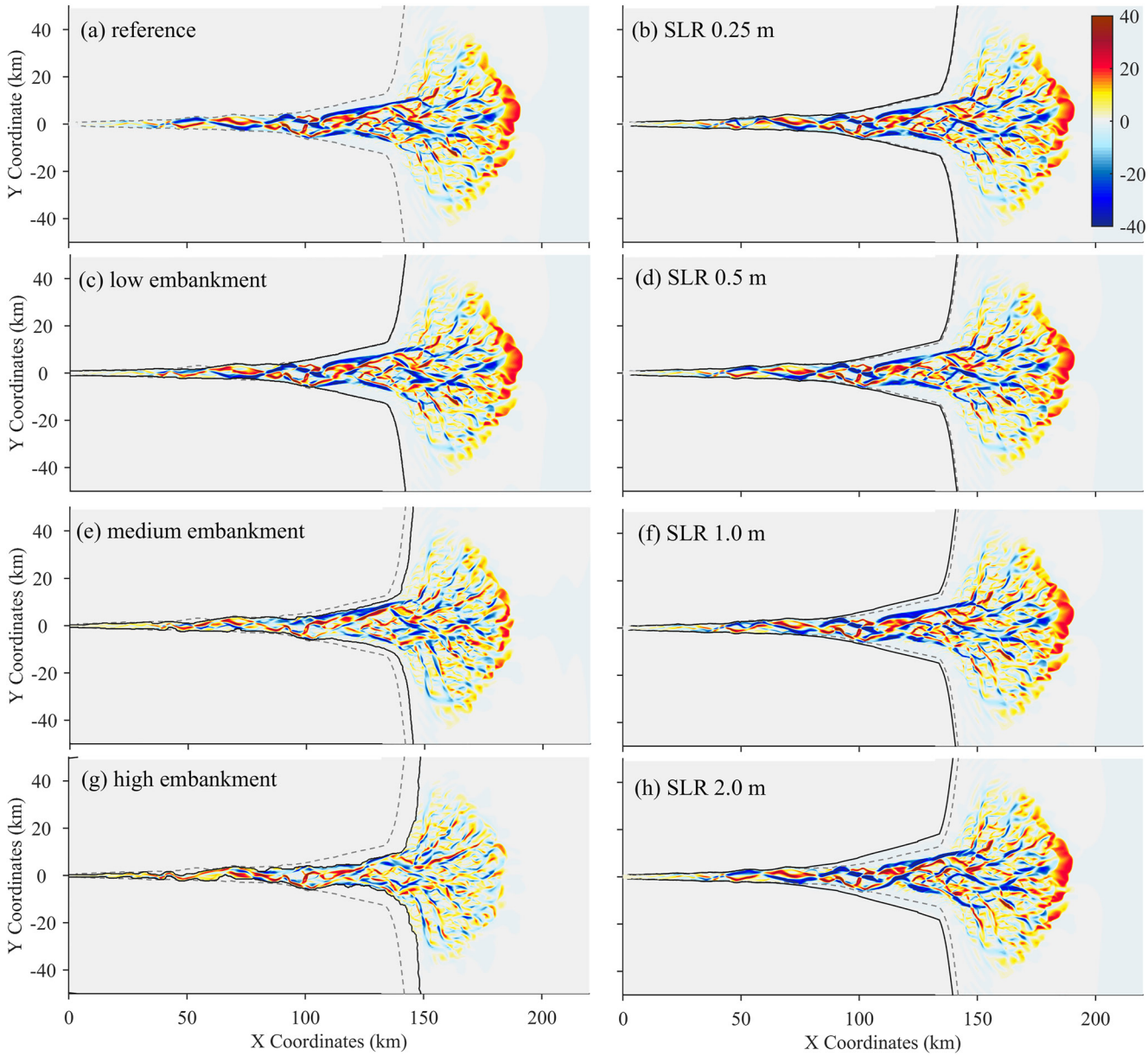

Figure 5. The erosion and deposition pattern in (a) the reference scenario (NE-noSLR), the scenarios considering sea-level rise (SLR) only of (b) 0.25 m (NE-SLR025), (d) 0.5 m (NE-SLR050), (f) 1.0 m (NE-SLR100) and (h) 2.0 m (NE-SLR200) and the scenarios considering tidal flat embankment only (c) low embankment (LM-noSLR), (e) medium embankment (ME-noSLR), and (g) high embankment (HE-noSLR). The dashed lines indicate the shorelines (high tide) in the reference scenario and the solid lines are the new shorelines in the SLR and embankment scenarios.

As a result, tidal wave distortion leads to a shorter rising tide duration than that of the falling tide (Table 2), suggesting changes in tidal asymmetry.

The cross-sectionally averaged current velocities at the mouth section (calculated by the cross-section integrated discharge divided by the cross-sectional area) decrease in magnitude in the embankment scenarios (see Figure S3 in Supporting Information SI). The peak ebb current velocities are larger than the peak flood current velocities in the scenarios without embankment, and this asymmetry reduces when tidal flat embankment is implemented. Furthermore, the peak flood currents become slightly larger than peak ebb currents in the high embankment scenarios. These changes suggest that tidal flat embankment can reduce ebb dominance, and even induce a switch to flood dominant tidal asymmetry.

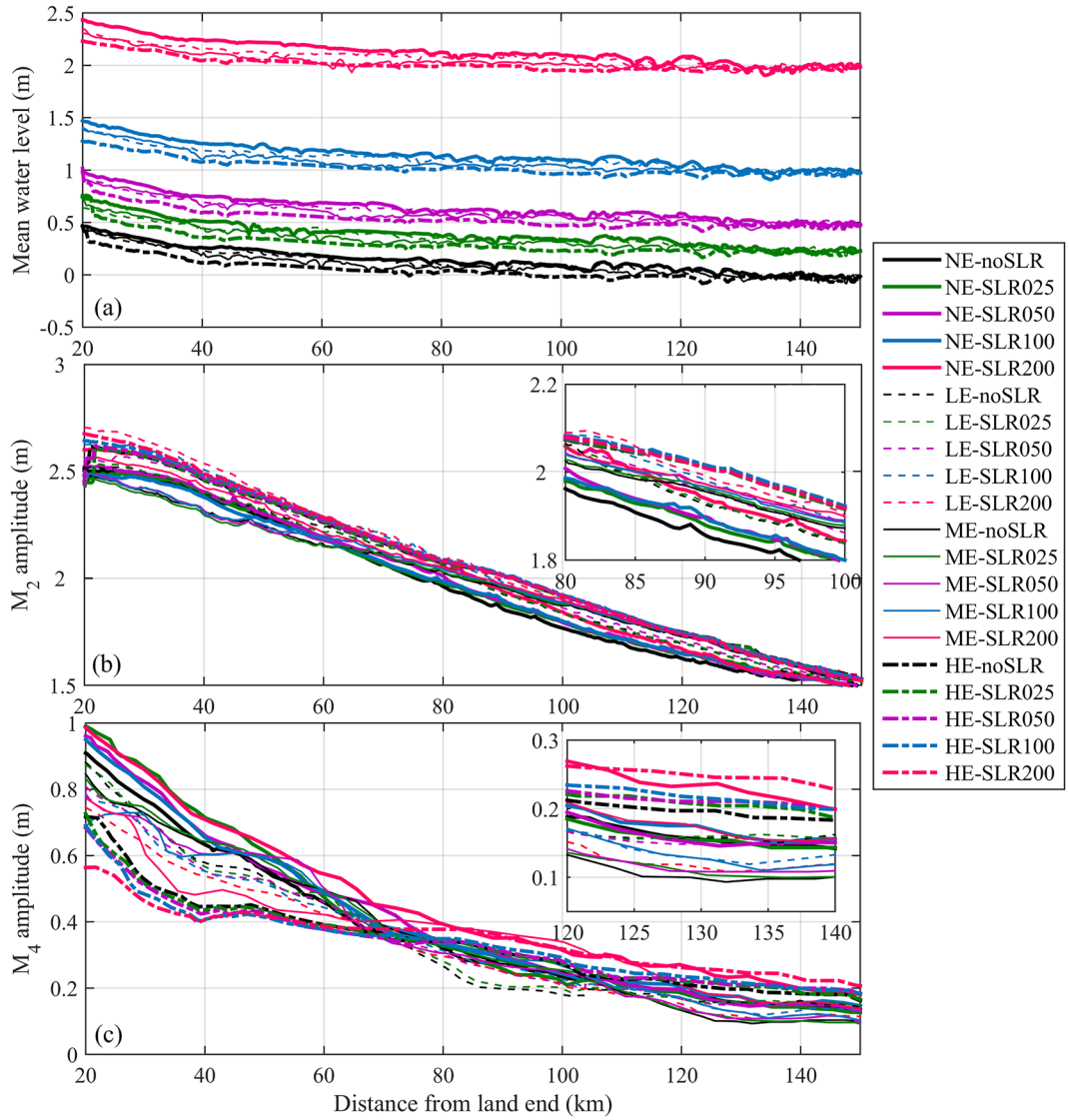

Figure 6. Changes of cross-sectionally averaged (a) mean water level, (b) M_2 amplitude, and (c) M_4 amplitude in the sensitivity scenarios considering sea-level rise and embankment based on the morphology at the end of 100-year simulation. The small plots in (b) and (c) were zoom-in views of the selected channel segment to demonstrate the differences.

The tidal prism of the basin increases over the 100-year in the reference case and SLR enlarges the increase, because of an increase in water depth, surface areas, cross-sectional areas, and intertidal storage volumes in response to lateral shoreline expansion (Figure S4 in Supporting Information SI). For instance, the tidal prism is 29% larger in the NE-SLR200 scenario compared to the reference case at the end of the 100-year simulation, that is, an increase from 6.32 to 8.15 km^3 (Table 2). Tidal flat embankment, however, reduces the tidal prism (Table 2), because of a loss in intertidal storage volume. For instance, the tidal prism is 30% smaller in the HE-noSLR scenario, that is, a decrease from 6.32 to 4.45 km^3 (Table 2). When both SLR and tidal flat embankment are considered, the SLR-induced changes in tidal prism decrease in magnitude with increasing degrees of embankment. The tidal prism even decreases after 30 years in the HE-noSLR, HE-SLR025, and HE-SLR050 scenarios (Figure S4d in Supporting Information SI), because of sediment import and channel deposition (see Section 3.3).

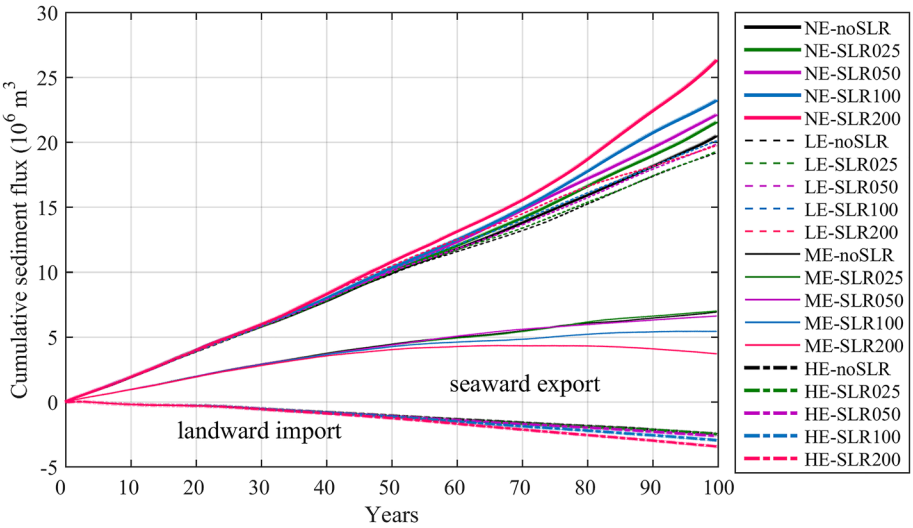

Figure 7. Changes of cumulative sediment flux at the mouth section over 100 years in all sensitivity simulations. Positive values indicate sediment export (seaward flux) and negative indicate sediment import (landward flux).

3.3. Sediment Flux Changes

We calculated the tidally averaged sediment flux at the mouth section of the tidal basin, that is, the interface between the inner basin and the outer sea, to indicate the sediment transport regime. The cumulative sediment flux at the mouth section is persistently seaward over the 100 years in the reference case (Figure 7), indicating a net sediment export. This seaward sediment flux is ascribed to stronger ebb currents than flood currents (Figures S3 and S4 in Supporting Information SI), due to the combined impact of the hydraulic storage of intertidal zone and a Stokes' return flow, as observed in similar tidal basins (Ridderinkhof et al., 2014; van der Wegen and Roelvink, 2008), although the rising tidal duration is shorter than that of the falling tide (Table 2).

In the absence of tidal flat embankment, SLR enlarges the sediment export and a higher SLR leads to larger sediment export (Figure 7). This is primarily the result of enhanced ebb dominance generated by increased storage volume under SLR. A larger tidal prism in the SLR-only scenarios may also contribute to the larger sediment export (Table 2). The impact of SLR also increases over time, when the mean sea level is adjusted with an exponential rate of SLR, that is, more significant impact in the last 50 years than in the first 50 years.

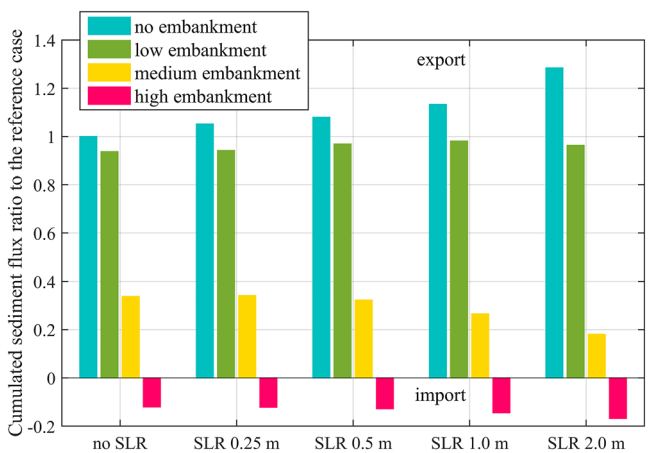

Figure 8. The ratio of the 100-year cumulated sediment flux at the mouth section in the sensitivity scenarios to that in the reference case. Positive values indicate sediment export (seaward flux) and negative ones indicate sediment import (landward flux).

In contrast, tidal flat embankment reduces the seaward sediment flux at the mouth. For instance, in the medium embankment scenarios (ME series), the cumulative sediment export reduces from 6.91×10^6 m^3 in ME-noSLR to 5.43×10^6 in ME-SLR100 and 3.70×10^6 m^3 in ME-SLR200 (Table 2). The cumulative sediment export in the ME-noSLR scenario is only one-third of that in the reference case. Moreover, a striking change from sediment export to sediment import occurs in the high embankment scenarios (Table 2 and Figures 7 and 8). The landward sediment flux (import) becomes larger under SLR (Figure 8), for example, increased from 2.47×10^6 m^3 in HE-noSLR to 3.44×10^6 m^3 in HE-SLR200 (Table 2). The landward sediment flux is ascribed to a larger maximal current velocity during the flood phase than the ebb phase (i.e., 1.2 versus. 1.1 m/s in the HE-noSLR scenario, Figure S3 in Supporting Information SI), and consequently, the cross-section integrated sediment flux has become significantly larger during flood tides than ebb tides (Figure S5 in Supporting Information SI). This is because sediment transport is proportional to a power function of velocity with an order larger than 3. Hence, even a small difference in current velocity differences induces a larger difference in sediment flux.

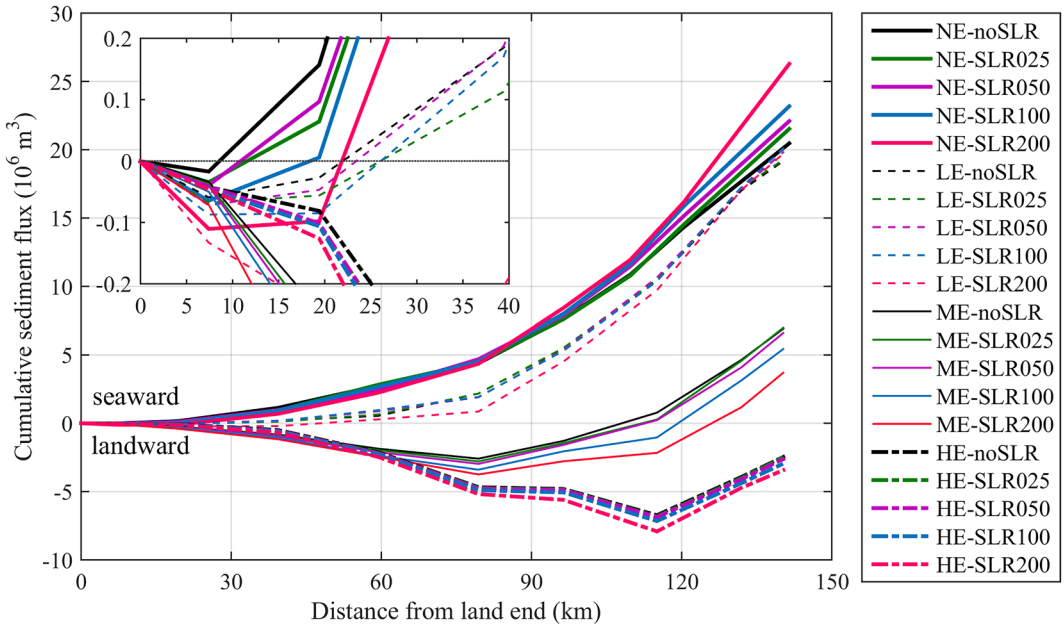

Figure 9. Streamwise variations of the cumulative sediment flux over 100 years in all scenarios. Positive values indicate sediment export (seaward flux) and negative indicate sediment import (landward flux). The zoom-in subplots show the landward sediment flux in the most landward region.

Overall, SLR enhances sediment export in the reference case and low embankment scenarios, but reduces the export in the medium embankment scenarios and enhances sediment import in the high embankment scenarios, whereas embankment predominantly reduces sediment export, even causing a shift to sediment import in the high embankment scenarios (Figure 8 and Table 2). The reduced sediment export and the shift to import explains the reduction in seaward progradation of the ebb-tidal delta, when compared with the reference case (e.g., ~6 km less on average in HE-SLR200 compared to NE-SLR200; see Figures 4d and 2i).

Spatially, the (cross-sectionally integrated) cumulative sediment transport is predominantly seaward inside the basin in the reference case, apart from some landward transport in the most landward segment of the channel (landward ~ km-20) (Figure 9), which explains the shoaling therein (see Figure S6 in Supporting Information SI). The magnitude of the cumulated sediment flux decreases in the landward direction in the reference case and low embankment scenarios. The magnitude becomes larger around the mouth but slightly smaller inside the basin under SLR, suggesting enlarged streamwise gradients. In the medium embankment scenarios, seaward sediment transport occupies the seaward segments of the basin (seaward km-115), while landward transport prevails in the other parts of the tidal basin (Figure 9), suggesting sediment transport divergence. Landward net sediment transport occurs throughout the tidal basin in the high embankment scenarios, with the largest magnitude occurring inside the basin (km-110), instead at the mouth.

The changes in the cross-sectionally integrated sediment flux are confirmed by the spatial distribution of the tidally averaged sediment transport vectors. The sediment transport flux prevails in the deep channels, and was smaller over shallower regions (Figure 10). Seaward flux predominates in the reference case both at the beginning and at the end of the 100-year simulation. However, it changes to become landward under the same bathymetry when a major portion of intertidal flats is reclaimed (Figure 10c). The landward flux persists after 100 years when considering both high embankment and SLR of 2.0 m (Figure 10d). In addition, we see circulations of the sediment transport flux in the high embankment scenarios, which may explain the smaller cross-sectionally averaged transport flux compared to the reference case.

The tidally averaged sediment transport may exhibit transitional changes within the 100 years in the medium and high embankment scenarios. The sediment export at the basin mouth changes into import after ~95 and ~80 years in the ME-SLR100 and ME-SLR200 scenarios, respectively (Figure 11d). This is consistent with the noted decline in the cumulative sediment flux (see Figure 7). The seaward sediment flux persists throughout the

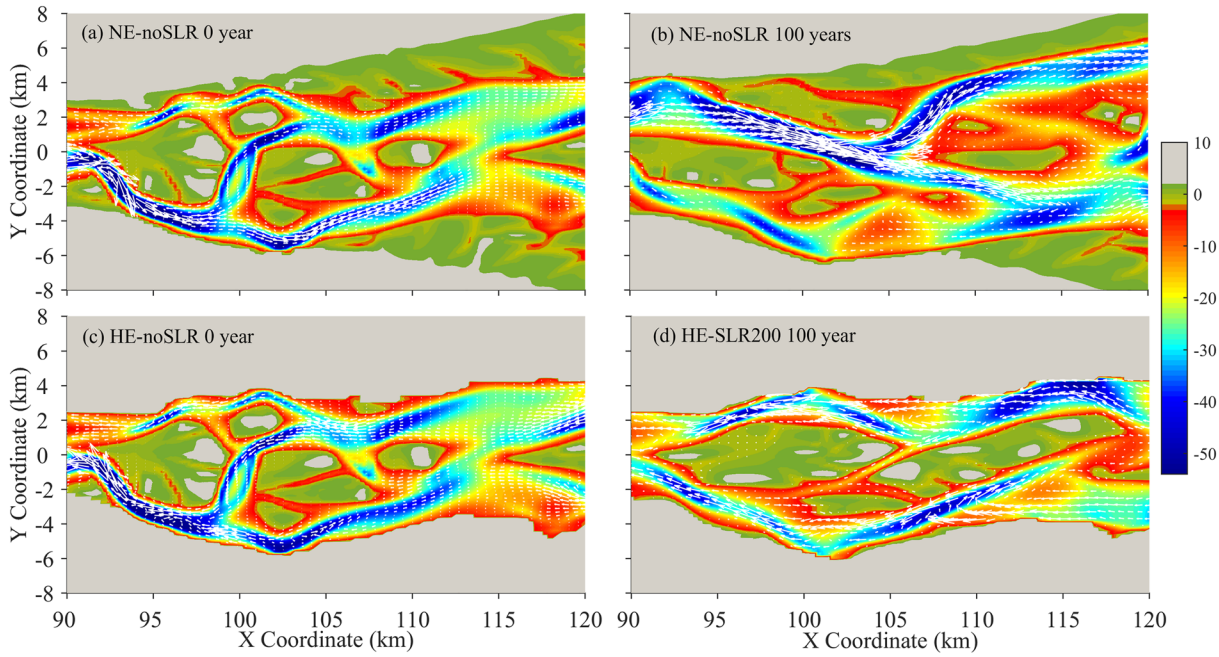

Figure 10. Distribution of the tidally averaged sediment transport vectors in a selected segment of the basin (km-90 to km-120) at the beginning and end of the 100-year simulations, with the bathymetry in the background: (a) NE-noSLR at the beginning, (b) NE-noSLR at the end, (c) HE-noSLR at the beginning, and (d) HE-SLR200 at the end. The length scale of the vectors in panel (c) and (d) is a third of that in panel (a) and (b).

basin and over the 100 years when a major portion of the intertidal flats is reclaimed (Figures 11e and 11f). The absolute magnitude and longitudinal gradients in sediment export reduced over time (except the scenarios considering SLR only), suggesting ongoing morphodynamic adaptation to restore equilibrium (Figure 11).

3.4. Basin Hypsometry Changes

The channel volume increased overtime in the reference case due to sediment export. SLR enhanced the increase, while embankment mitigated the increase. A high embankment rate however induced a decrease in channel volume due to sediment import. The impact of SLR on the channel volume became less significant when considering low and medium embankment. SLR slowed down the decrease in channel volume in the high embankment scenarios and a high SLR caused a shift to increase after the first ~20 years (Figure 12).

Changes in intertidal storage volume reflected the hypsometric effect on tidal asymmetry. The intertidal storage volume slightly increased overtime in the reference case, and SLR enhanced the increase (Figure 12b). In the presence of low embankment, the intertidal storage volume slightly decreased over time when there was no SLR or SLR of 0.25 m, but increased for SLR >1.0 m (Figures 12c and 12d). The decrease in the medium embankment scenarios (Figure 12f) and the increase in the high embankment scenarios (Figure 12h), are, however, only marginally affected by SLR. Moreover, SLR alleviates the reduction in intertidal storage volume in the low embankment scenarios, whist a higher rate of SLR reverses the reduction.

The intertidal flat area within the tidal basin and over the ebb-tidal delta was calculated to check how tidal flat evolution responded to SLR and embankment. The reclaimed floodplains in the embankment scenarios were excluded in the calculations, while the newly established flats, formed by the submerged low-lying floodplains, were included in the SLR scenarios. The adjustment of high water and low water and the intertidal range are considered with rising sea levels. While the intertidal areas within the tidal basin change little over the 100 years in the reference case, SLR slowed down the decrease and a high SLR rate even causes an increase due to lateral shoreline migration and the creation of new flats (Figure 13a). These changes are a consequence of the additional accommodation space created on the surrounding floodplain and hence depend on the local topography. In these simulations they reflect the assumption made about the slope of the surrounding land.

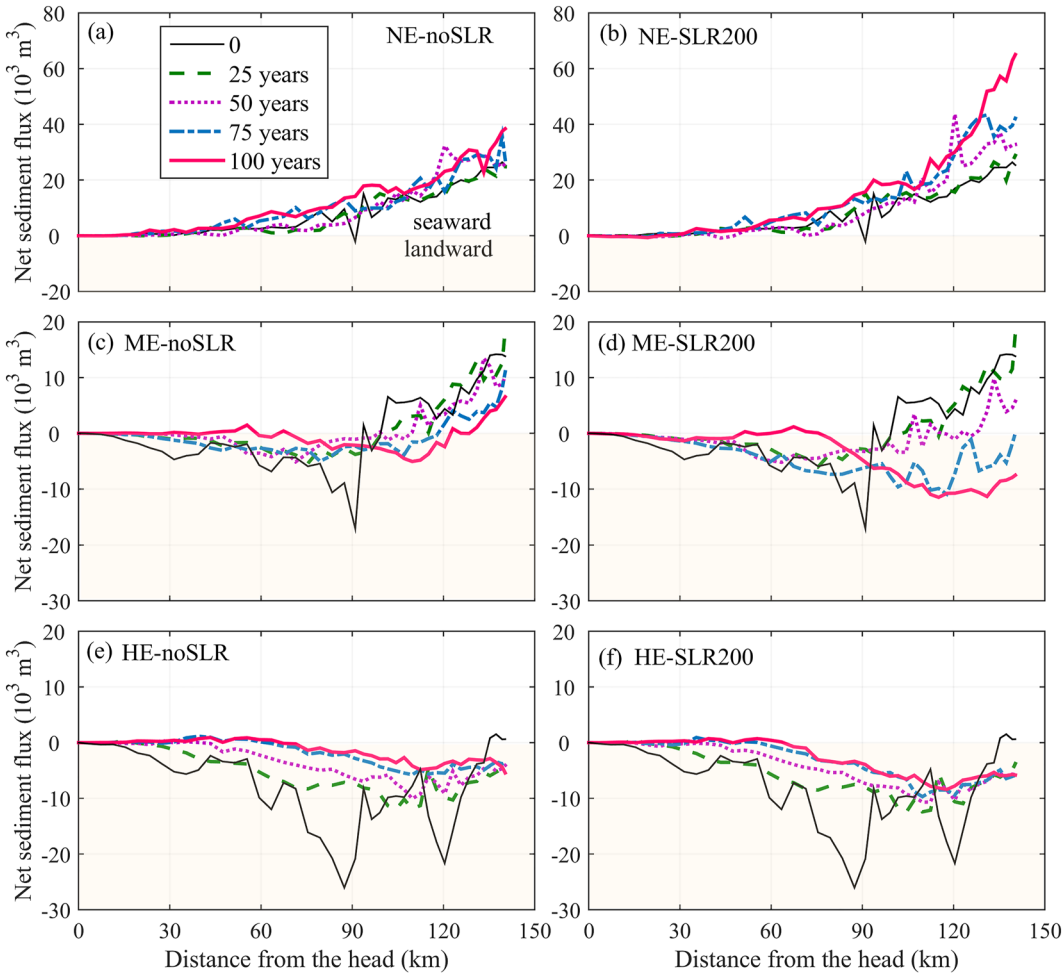

Figure 11. Streamwise variations of the tidally averaged sediment flux after 0, 25, 50, 75, and 100 morphodynamic years in the (a) NE-noSLR, (b) NE-SLR200, (c) ME-noSLR, (d) ME-SLR200, (e) HE-noSLR, and (f) HE-SLR200 scenarios. Positive value indicates seaward flux and negative value indicates landward flux. Note that the scales of the *y*-axis in (a) and (b) are larger than that in (c)–(f).

At the beginning of the sensitivity simulations, embankment reduces the intertidal area, that is, by 4%, 49%, and 76% in the low, medium, and high embankment scenarios, respectively. Over the following 100 years, the intertidal area reduces in the low and medium embankment scenarios, due to the persistent sediment export (despite the slight increase in the initial 20 years; Figure 13c), but increases in the high embankment scenarios because of sediment import (Figure 13d). The temporal increase in intertidal flats in the high embankment scenarios suggests that tidal flat accretion (and expansion) may keep pace with SLR. However, it should be noted that the rate of accretion is relatively small and slow. Hence, the net intertidal area at the end of the 100 years is still much smaller than for the reference case.

The hydraulic depth of the main channel (i.e., the ratio of the channel volume to surface area at mean water level) increases over time in the reference scenario, because of sediment export (see Figure S7 in Supporting Information SI). The increase becomes smaller under SLR, suggesting that SLR induces a larger increase in surface area than volume. Tidal flat embankment results in an increase of the hydraulic depth of the main channel, particularly in the high embankment scenarios in which the hydraulic depth reduces over time. The hydraulic depth of the intertidal zone (i.e., intertidal volume divided by intertidal area) increases significantly in response to SLR and in the presence of embankment, due to the increase in intertidal storage volume and the decrease in intertidal flat area. This increase becomes larger when embankment is implemented, although the temporal changes remain small in the embankment scenarios when there was no SLR. However, for the SLR scenarios, a larger hydraulic depth was establishes in the intertidal zone because the planimetric area is constrained, while the water depth

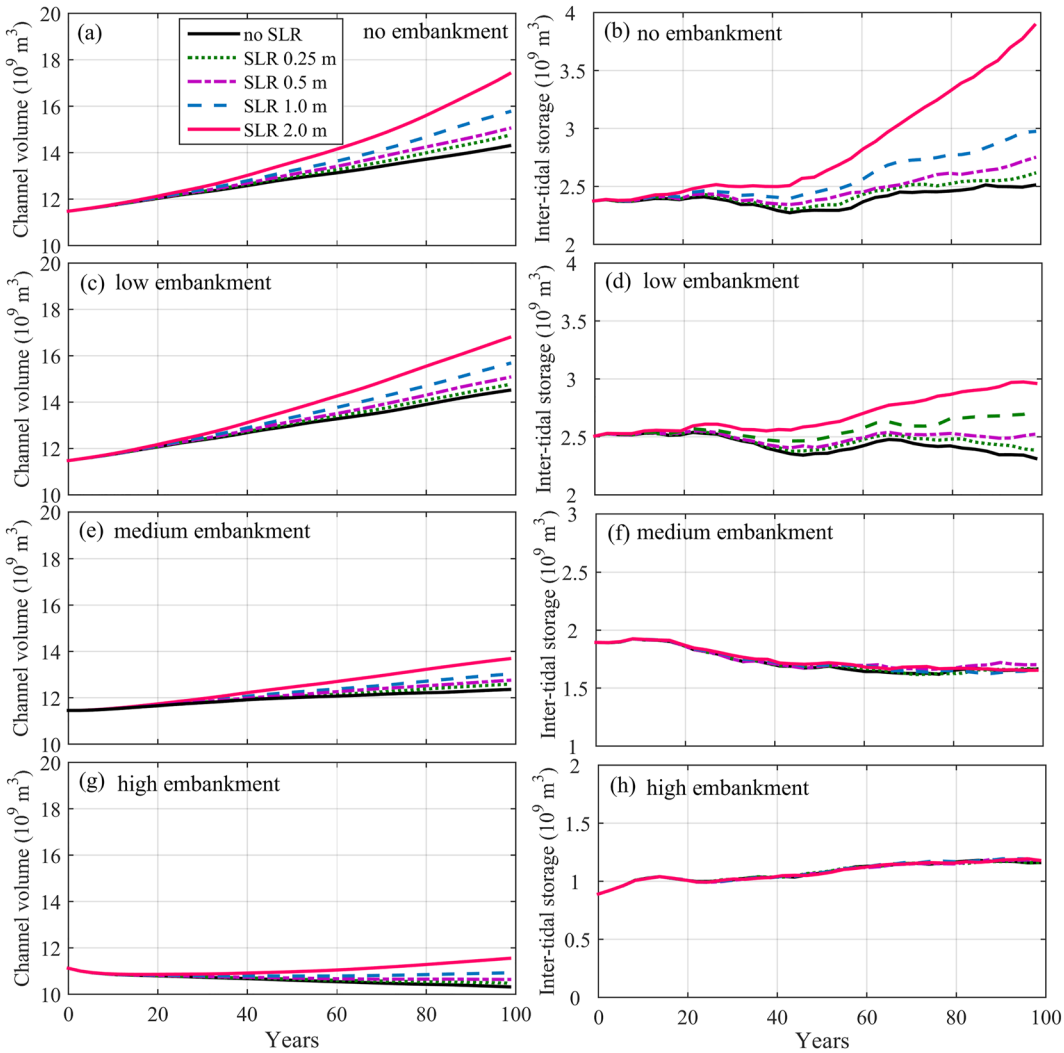

Figure 12. Temporal changes in (a, c, e, g) channel volume below mean water level and (b, d, f, h) intertidal storage volume of the basin in the no (a), (b), low (c), (d), medium (e), (f) and high (g), (h) embankment scenarios.

increased. The increase in hydraulic depth of the main channel is more significant when reclaiming the tidal flats below the mean sea level, while the increase in hydraulic depth of the intertidal zone is more significant when removing the tidal flats above the mean sea level.

The intertidal flat area in the ebb-tidal delta increases over time in the reference case, due to sediment supply from the landward tidal basin (Figure 14a). When SLR is <1.0 m, the increase rate in intertidal area reduces and switches to a decrease when SLR is 1.0 and 2.0 m. This implies tidal flat accretion at smaller rates under SLR conditions. Similar increasing or decreasing trends are observed in the scenarios considering tidal flat embankment (Figures 14b–14d). Overall, these results suggest that vertical tidal flat accretion over the ebb-tidal delta fails to match the rate of SLR. It is noteworthy that the intertidal flat area still increases over time in the ebb-tidal delta for the HE-noSLR scenario (considering landward residual sediment transport), which is ascribed to sediment redistribution resulting from subtidal channel erosion and flat accretion as indicated by the hypsometry changes (Figure S8 in Supporting Information SI).

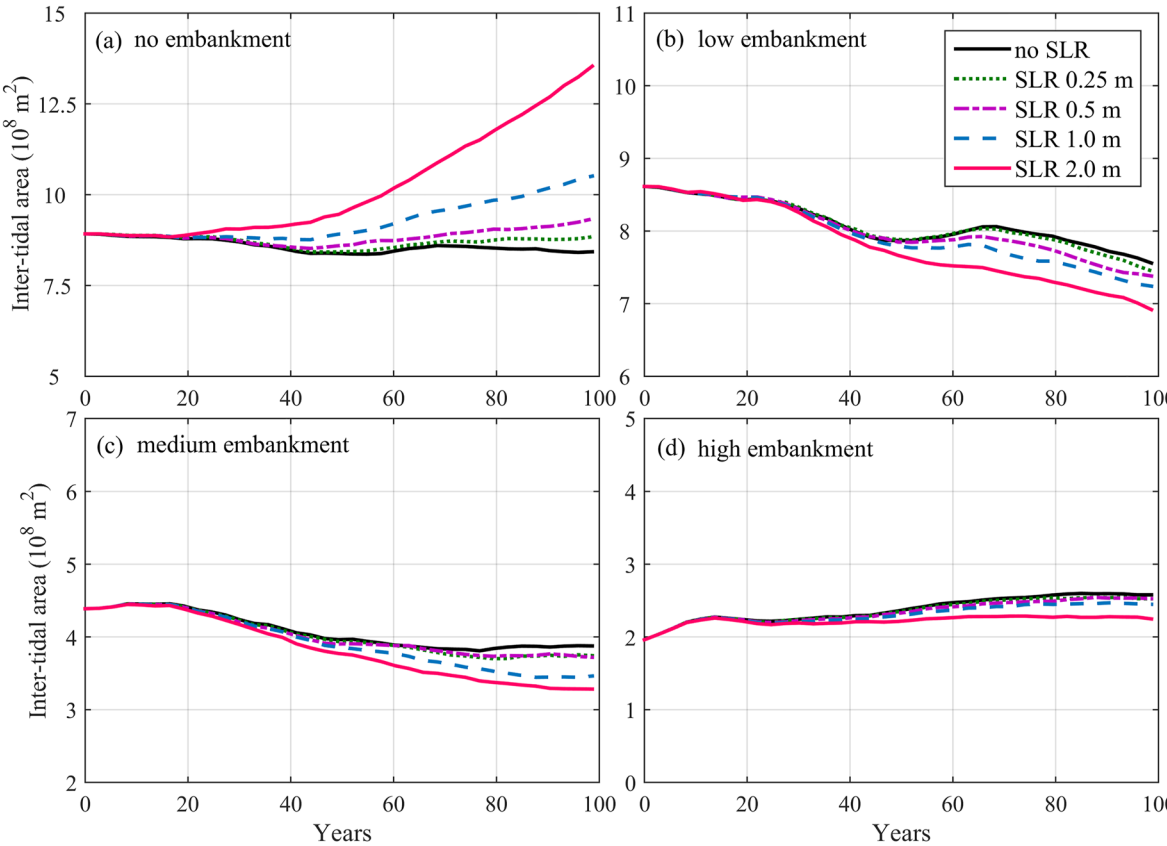

Figure 13. Temporal changes in intertidal flat area inside the tidal basin over 100 years considering sea-level rise in the (a) no, (b) low, (c) medium, and (d) high embankment scenarios. Note that the scale of the *y*-axis in panels (b)–(d) is different to panel (a).

4. Discussion

4.1. Impact of Tidal Flat Reclamation

The model results highlighted how reclamation of tidal flats affects the large-scale hydro-morphodynamics besides the direct consequence in reducing tidal flat area. First, loss of tidal flats affects tidal evolution (Holleman & Stacey, 2014; Pelling et al., 2013; Talke & Jay, 2020). Embankment narrows the tidal channel and alters its width convergence, which exerts a feedback impact on tidal wave propagation. Intertidal flats and subtidal regions are known as sinks of momentum and energy and thus influence tidal damping (Speer & Aubrey, 1985). The presence of tidal flats and subtidal areas change the effective depth and convergence (Ensing et al., 2015; Jay, 1991). Loss of tidal flats explains the more amplified tides, as found in this study. Similar changes are observed and modeled in natural tidal basins. For instance, Holleman and Stacey (2014) modeled a 1 m SLR and showed that this amplified the tides in San Francisco Bay, when the shoreline was kept rigid, but decreased tides when flooding of overland floodplains was allowed. Ensing et al. (2015) suggested that the increase in tidal amplitude induced by SLR would be decreased if overland flooding occurred in the Ems Estuary. Similar changes were modeled in the Delaware Estuary (Hall et al., 2013; Lee et al., 2017; Ross et al., 2017) and in the Chesapeake Bay (Du et al., 2018; Lee et al., 2017), indicating the strong impact of tidal flat loss on tidal dynamics.

A second impact of tidal flat reclamation is on tidal asymmetry and the tidally averaged sediment transport. Tidal flat embankment sharply reduces the planimetric area of the tidal basin, the cross-sectional area, as well as the intertidal flat area and associated storage volume. The reduction in cross-sectional area may be at a larger rate than the increase caused by SLR. Hence, a reduction in tidal prism is partially responsible for the reduced sediment export in the embankment scenarios. Moreover, the reduction of intertidal storage volume, in the embankment scenarios, mitigates the ebb dominance and sediment export. In the extreme case when a major portion of the intertidal flats is reclaimed (the high embankment scenarios), the hypsometric effect of intertidal storage

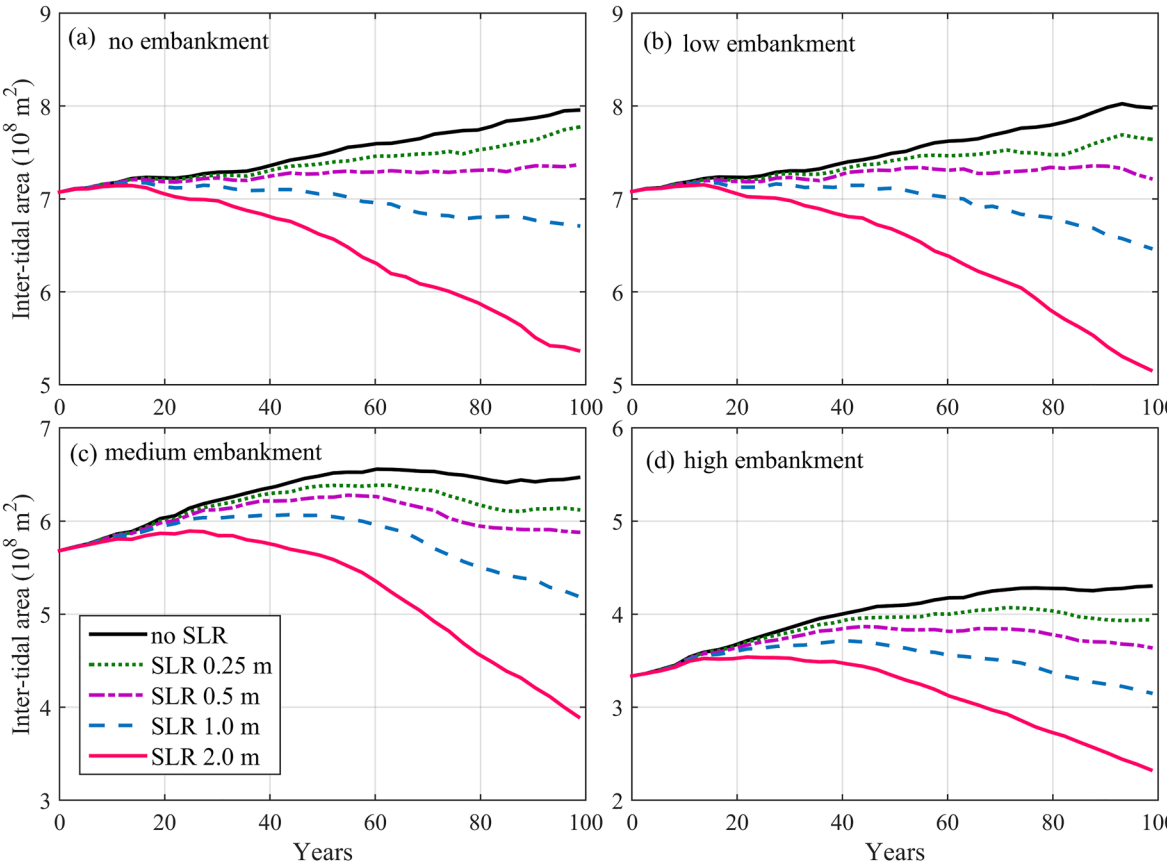

Figure 14. Temporal changes in intertidal flat area over the ebb-tidal delta considering sea-level rise in the (a) no, (b) low, (c) medium, and (d) high embankment scenarios.

becomes negligible. As a result, stronger flood currents and shorter rising tides substantially change the tidal asymmetry, resulting in sediment import.

The third significant impact of tidal flat embankment is on the medium-to long-term morphology. While SLR may increase intertidal flat area by submerging low-lying floodplains, the dikes used for tidal flat reclamation prevent lateral shoreline migration, resulting in a decrease in intertidal area. Although sediment import in the high embankment scenarios mitigates the intertidal flat loss to some degree, this mitigation effect is slow when compared with the direct tidal flat loss to reclamation. Thus tidal flat area at the end of the 100-year simulations is still much smaller compared to the reference case (see Figure 13).

As regards to the ebb-tidal delta, tidal flat area does not necessarily increase under sediment export because of the differences between the vertical flat accretion rate and SLR rate. The reduced sediment export in the embankment scenarios leads to a decline in sediment supply to the ebb-tidal delta. The shift to sediment import in the high embankment scenarios implies erosion of the ebb-tidal delta, given that there is no other sediment supply from the sea. This explains why the ebb-tidal delta progradation is much slower in the embankment scenarios. These changes further illustrate how the tidal basin and the ebb-tidal delta behave as an inherently connected morphodynamic system, that is, changes within the tidal basin exert far-field impact on the outer ebb-tidal delta.

The hydro-morphodynamic impact of SLR varies with the degrees of tidal flat embankment. The shift from sediment export to import in the last decades in the ME-SLR100 and ME-SLR200 scenarios and the persistent sediment import in the HE scenarios indicates the combined influences of SLR and embankment. The regime shift is explained by a feedback mechanism between hydrodynamics and morphology. On the one hand, the phase differences between tidal water levels and tidal currents remain nearly the same between the SLR and embankment scenarios. However, SLR increases the water depth, which causes a reduction in the strength of the Stokes return flow because it is distributed over a larger water column (Ridderinkhof et al., 2014). On the other hand,

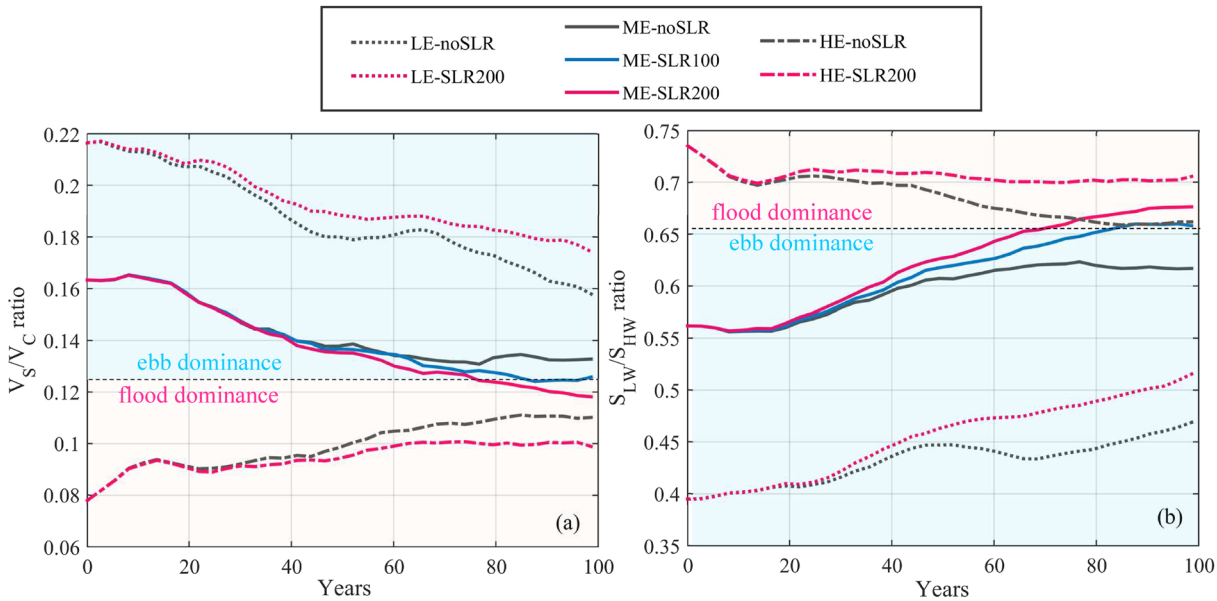

Figure 15. Changes of (a) V_s/V_c and (b) S_{lw}/S_{hw} in the tidal basin over 100 years in the selected scenarios considering sea-level rise and embankment.

the ratio of the intertidal storage volume to channel volume (V_S/V_C) and the ratio of the low water planimetric area to high water planimetric area (S_{LW}/S_{HW}), two indicators of the hydraulic storage impact of intertidal zones, reach thresholds of ~0.125 and ~0.66, respectively, when the shift occurs (Figure 15). The threshold for V_S/V_C is consistent with the threshold derived from idealized modeling stimulations in 1D (Friedrichs & Aubrey, 1988) and 2D circumstances (Zhou et al., 2018). A reduction in V_S/V_C and an increase in S_{LW}/S_{HW} indicate a loss of intertidal area and storage volume, which is particularly the case in the scenarios with large SLR and high embankment. Both changes resulted in a reduction in ebb dominance and a shift to flood dominance takes place when the thresholds are passed.

We see that the hydro-morphodynamic impact of embankment is much more substantial than that of SLR. SLR exacerbates the impact of tidal flat embankment. The tidal prism decreases with embankment. Both the sediment transport magnitude and the residual transport flux decrease with embankment. The SLR-induced changes in tidal flat areas, channel volumes, and intertidal storage volumes become smaller with increasing extent of embankment (low to high). These results suggest that embankment reduces the system's morphodynamic activity and adjustment capacity in response to SLR. Inundation and erosion of the low-lying floodplains under rising sea levels provides a buffering capacity in counteracting SLR, whereas tidal flat embankment prevents the channels from expanding laterally, thus depriving the system from using its morphodynamic feedback mechanism to adapt to SLR. This influence is much more profound when SLR is high and embankment is extensive. This hydro-morphodynamic feedback mechanism may explain the enhanced flood dominance in the North Branch of Changjiang Delta in response to extensive tidal flat reclamation (Guo et al., 2021).

4.2. Model Limitations and Future Research Needs

As explained in the model setting section, we adopted a schematized model that focuses on the impact of tidal flat embankment and SLR in tide-dominated convergent basins. This ignores the influence of river flow, salinity gradients, wind-waves, sediment heterogeneity and variations in sediment supply that are likely to play a role in the morphological response of this type of system. River flow is expected to provide an additional source of sediment supply and to enhance seaward sediment transport (Guo et al., 2014), which can counter the landward transport induced by embankment. The gravitational circulations created by the interactions between fresh and saline water can cause landward sediment transport near bottom, enhancing sediment trapping within estuaries (Geyer et al., 2001; Sommerfield & Wong, 2011). To provide some preliminary impression of these excluded forcing conditions on the morphodynamics in this work, we ran a few extra simulations considering river discharge and sediment grading (Figures S9-S11 in Supporting Information SI). Including a small river discharge and

3-dimensional processes, Figure S9b in Supporting Information SI, made little difference to the channel pattern and morphodynamic development because the amplified tide and large tidal discharge predominate. A larger river discharge would damp the incoming tide and enhance the ebb-tidal currents and associated seaward sediment transport (Figure S9c in Supporting Information SI). It would therefore enhance the sediment export and possibly mitigate the sediment import in the high embankment case. Moreover, including a river discharge introduces additional fluvial sediment supply to the system. As a result, more intertidal flats are likely to form in the mouth zone of the tidal basin and the ebb-tidal delta is more likely to prograde seaward. Further in-depth investigation is still needed to determine the potential impact of the near-bottom landward sediment transport driven by density circulation under varying river-tidal forcing conditions (Olabarrieta et al., 2018; Zhou et al., 2020).

Varying the sediment grain size and the addition of a mud fraction also have a distinct influence. Adding mud to tidal estuaries tends to introduce more variability in the morphodynamic response, for example, landward flux of mud in the Humber Estuary (Townend & Whitehead, 2003) and Western Scheldt Estuary (Dam et al., 2016), and less bifurcated channels (Edmonds & Slingerland, 2010), because fine sediment transport involves more dynamic processes such as slack water asymmetry, and settling and sour lag effects (de Swart & Zimmerman, 2009). In this work, the additional simulations considering sediment with smaller or larger grain size (64 and 300 μm) exhibited very similar results, while differing primarily in the morphodynamic evolution speed (Figure S10 in Supporting Information SI). The sediment transport rate is larger and the associated morphodynamic development is faster under smaller grain size, given that sediment transport increases with decreasing grain size (Engelund & Hansen, 1967). Similar findings have been reported in other studies (e.g., Grasso et al., 2021), and this topic merits further in-depth investigation. In contrast, the channels inside the tidal basin become more regularly meandering, the tidal flats become more extensive, and the distributary channels over the ebb-tidal delta become less braided when adding 10% mud to the noncohesive sand (Figure S11 in Supporting Information SI). Note that the morphodynamic results are very sensitive to the parameter settings of cohesive sediment, such as the percentage of mud compared to sand, the critical erosion and deposition shear stresses (and their spatial distribution), the settling velocity, and the initial thickness of mud on the bed (Olabarrieta et al., 2018; Zhou et al., 2020). Hence, the role of mud transport on large-scale estuarine and deltaic morphodynamics still merits further examination.

Furthermore, the excluded wind-waves may enhance sediment resuspension and help to stimulate sand bar merging and reduce the number of distributary channels in the ebb-tidal delta, as have been reported over river deltas (Geleynse et al., 2011) and tidal basins (Elmilady et al., 2022). Future study is also needed regarding the sensitivity to the lateral tidal flat profile slope, quantification of the morphodynamic adaptation scale, and the morphodynamic equilibrium restoration under the sediment import regime.

This study focuses on the physical processes, while biophysical interaction and the coupled eco-morphodynamic evolution may further highlight the value of wetland conservation in response to SLR. The vertical accretion rate of saltmarshes is larger than that over bare flats because of enhanced sediment trapping within the vegetation canopy (Fagherazzi et al., 2012; Kirwan et al., 2016). Moreover, vegetated tidal flats tend to have a larger erosion resistance. Hence, considering vegetation may reduce supra-tidal erosion and the sediment availability compared to the reference case. Accumulation of underground organic matter may further help intertidal habitat survival in response to SLR (Thorne et al., 2018). At a 100-year time scale, vegetation may also migrate landward to higher land in accord with shoreline expansion (Fagherazzi et al., 2019). Embankment of tidal flats deprives tidal systems of such adaptation capacity, capping ecosystem services, and in some cases, exacerbating the flood risk. Studying the interaction and mutual evolution between morphodynamic and bio- and ecological processes has received increasing research interest (Gourgue et al., 2021; Murray et al., 2008). It has led to a mindset change toward nature-based solution in coastal management, which meets the management objectives of tidal wetland ecosystem conservation and defense against erosion and flooding (Temmerman et al., 2013).

4.3. Implications for Management

This study highlights some of the likely long-term hydro-morphodynamic impact of large-scale tidal flat reclamation in tidal systems. System-scale morphodynamic adaptation is essentially slow when compared with the hydrodynamic response to SLR and tidal flat embankment; hence, such long-term impact has generally been understudied and underestimated. To indicate whether new morphodynamic equilibrium was being approached over the 100-year simulation, we examine the temporal variations of tidal prism (P) and cross-sectional area (A) at the mouth section (Figure 16). This shows that tidal flat embankment reduces the tidal prism at the

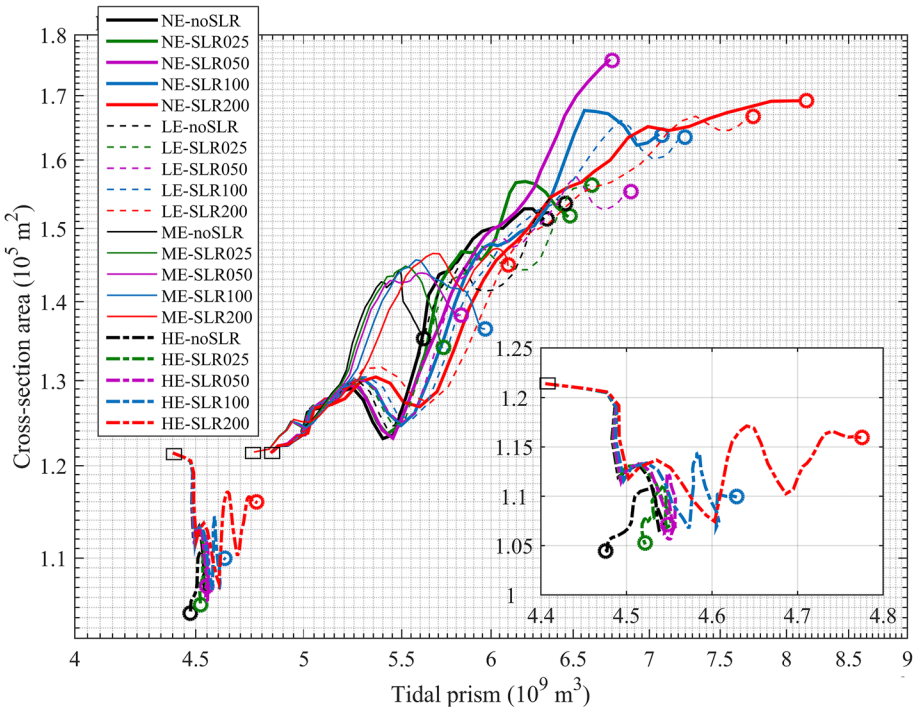

Figure 16. The temporal variations in tidal prism and cross-section area at the basin mouth for all scenarios. The subplot highlights a zoom-in view of the high embankment scenarios. The squares and circles indicate the results at the beginning and end of the 100-year simulations, respectively.

beginning, but the magnitude of the changes remain small compared to the changes caused by the subsequent hydro-morphodynamic adaptation. Both tidal prism and cross-section area increase in the none, low, and medium embankment scenarios, whereas the high embankment scenarios exhibited an increase in tidal prism but a decrease in cross-sectional area. This suggests that the high embankment scenarios are seeking a new cross-sectional area to match the reduced tidal prism at the beginning. The end state of the HE scenarios considering SLR then show a small increase in tidal prism and cross-sectional area relative to the HE-noSLR case. Furthermore, the oscillation in the progression toward a new equilibrium is more pronounced in the medium and high embankment scenarios, seemingly in accordance with the more dramatic modification of the morphology at the beginning. The oscillation is, however, consistent with previous arguments made by Dronkers (1986) and Pethick (1994) that tidal systems close to equilibrium may switch between flood and ebb dominance. Overall, the end state of all scenarios, with the exception of NE-SLR050, converge to a gently curving line in the P-A plot, suggesting that a systematic morphodynamic adaptation has been captured. Even though, the hydro-morphodynamic adaptation may continue after the 100-year simulation used in this study, before a static equilibrium is approached.

When interpreting these findings, it is important to note that the time scale in the model may not be exactly as that in nature, due to the total sediment load transport formula. Nonetheless, the findings provide an initial insight into the potential long-term implications of reclamation. Such an understanding of the system behavior, at large space and long timescales, is essential for successful coastal development and management.

Although the schematized model system in this study is not intended to represent any specific system in nature, the findings about the impact of embankment under SLR can still be informative for management of actual tidal basins and estuaries. The model results suggest that the coupled tidal basin-ebb delta system is more likely to drown under SLR when embankment is implemented (Figure 17). Tidal changes induced by embankment have consequent impact on erosion, flooding risk and ecosystems (Talke & Jay, 2020). Embanked tidal landscapes might have a higher flood vulnerability and lower flood resilience compared with the natural landscape, because the embanked regions are deprived of sedimentation from overwash events during high tide, whereas compaction of sedimentation and subsidence reduces their elevation (Auerbach et al., 2015; Hoitink et al., 2020). In addition, embankment of low-lying floodplains prevents marine transgression of the tidal basin and the associated

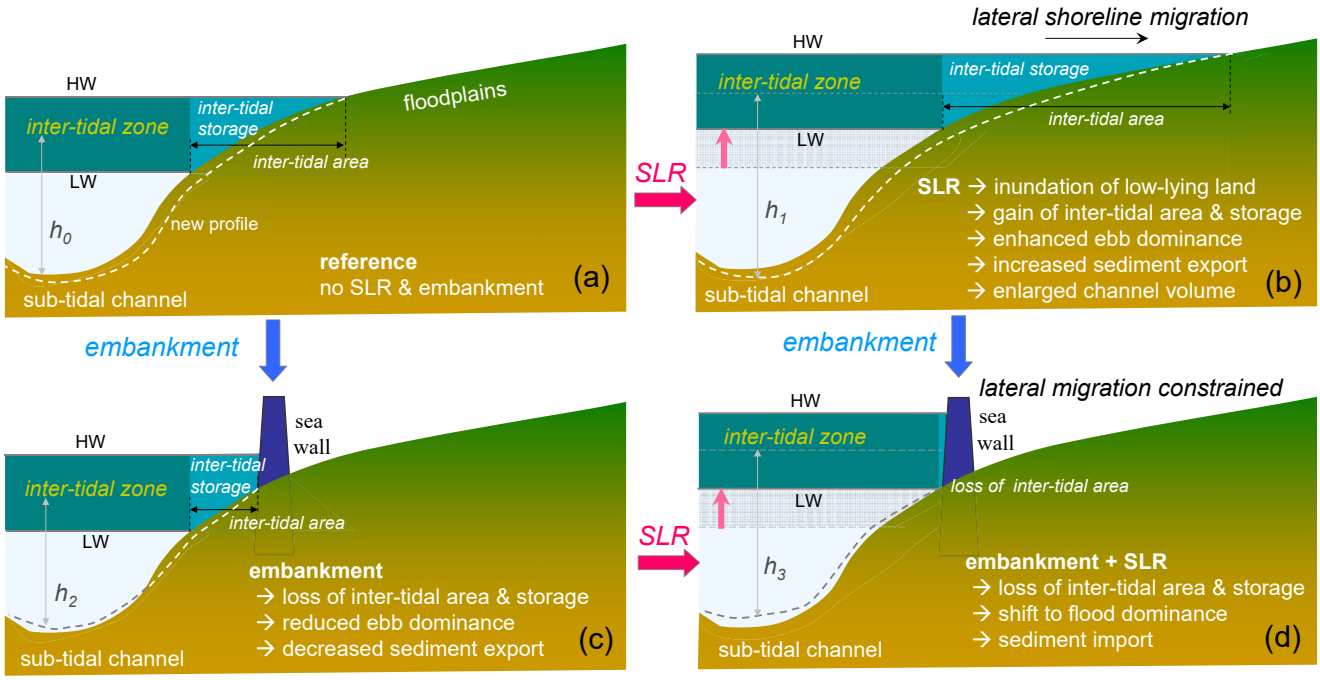

Figure 17. Conceptual sketches showing changes of the half cross-section profile (a) in the reference case, (b) (high) sea-level rise (SLR) scenario, (c) (medium) embankment scenario, and (d) combined embankment and SLR. LW and HW indicate low water and high water, respectively.

lateral expansion, thus constraining the system to adapt to external changes (Townend et al., 2021). The outsized influence of tidal flat embankment on tides and morphodynamic evolution suggests that it may be feasible to reverse the undesirable outcomes, for example, managed retreat (Townend & Pethick, 2002), thereby mitigating some of the future effects of climate change. For example, Orton et al. (2015) suggested that returning to historical depths would provide protection against future SLR in Jamaica Bay in New York harbor. Restoring tidal inundation by breaching embankment was thought to facilitate tidal flat recovery and, in some cases, mitigate the flooding risk (Auerbach et al., 2015; Townend & Pethick, 2002). The ecosystem services provided by flats and marshes can often be sufficient to justify coastal realignment in tidal basins and estuaries by breaching dikes and returning floodplains to nature to be flooded (Luisetti et al., 2014), thereby restoring some of the natural resilience to SLR (Orton et al., 2015; Xu et al., 2019).

This modeling study suggests that removing a major portion of intertidal flats within tide-dominated basins induces a landward sediment flux and channel deposition. It thus confirms the hypothesis that the extensive reclamation in the North Branch of the Changjiang Delta played a role in reinforcing sediment import and the channel aggradations (Guo et al., 2021). While sediment import is to the advantage of tidal basins and estuaries to counteract the drowning impact of SLR in general, persistent import and fast sedimentation in the North Branch, however, raises another management concern regarding channel shrinkage and significant loss of channel volume, possibly leading to channel extinction in the long term. Allowing tidal flats to accrete and expand under sediment import and SLR, instead of progressively reclaiming them, is expected to slow down sediment import and may eventually lead to an approach toward a new hydro-morphodynamic equilibrium.

5. Conclusions

In this study, we deployed a numerical model to explore the centennial morphodynamic evolution of a schematized tidal basin in response to SLR and tidal flat embankment. We found that sediment export at the mouth of the tidal basin in the reference case increases with SLR, but decreases with increasing degree of embankment. Tidal flat embankment reduces sediment export at a much larger rate than SLR and the loss of a major portion of intertidal flats causes a switch from sediment export to import. As a result of SLR and embankment, the tidal flat area and storage volume decreases but at different rates over time in the different scenarios. The morphodynamic

changes and adjustment are explained by the altered tidal dynamics and the competing effect between tidal wave deformation and intertidal storage effect.

The modeled tidal basin-ebb-tidal delta system exhibits resilience to SLR by making new accommodation space and sediment supply, and internal sediment redistribution. However, large-scale reclamation of intertidal flats significantly alters the system's hydro-morphodynamic adaptation at the decadal to centennial time scales, by (a) constraining sediment supply from bank erosion under rising sea level, (b) reducing the buffering capacity, due to sediment redistribution, within the system, and (c) altering the ebb dominance and sediment flushing to the sea (reduced sediment trapping effects) due to the removal of the tidal flats. The findings in this study indicates that restoring intertidal flats and low-lying floodplains for tide-dominated estuaries and basins has substantial benefit in preserving the system's own resilience to external changes like SLR, and lends support to the management paradigm of leaving room for nature instead of diking and fighting against nature.

Data Availability Statement

This modeling study used the open-source code Delft3D (version 4.04.01) [Software], developed by Deltares, which can be downloaded from https://oss.deltares.nl/web/delft3d/source-code. The two-dimensional model setting files are available at Figshare via https://doi.org/10.6084/m9.figshare.19703428.

Acknowledgments
This work is financially supported by the Ministry of Science and Technology, P.R. China (MOST) (No. 2016YFE0133700) and Royal Netherlands Academy of Arts and Sciences (KNAW) (No. PSA-SA-E−02), and also partly by Natural Science Foundation of China (Nos. 51739005, U2040216, 41876091), and Shanghai Committee of Science and Technology (No. 20DZ1204700).

References

Allen, J. R. L. (1990). The severn estuary of southwest Britain: Its retreat under marine transgression, and fine sediment regime. *Sedimentary Geology*, *66*(1–2), 13–28.

Auerbach, L. W., Goodbred, S. L., Mondal, D. R., Wilson, C. A., Ahmed, K. R., Roy, K., et al. (2015). Flood risk of natural and embanked landscapes on the Ganges-Brahmaputra tidal delta plain. *Nature Climate Change*, *5*, 153–157. https://doi.org/10.1038/nclimate2472

Best, U. S. N., van der Wegen, M., Dirkstra, J., Willemsen, P. W. J. M., Borsje, B. W., & Roelvink, D. J. A. (2018). Do salt marshes survive sea level rise? Modeling wave action, morphodynamics and vegetation dynamics. *Environmental Modelling & Software*, *109*, 152–166. https://doi.org/10.1016/j.envsoft.2018.08.004

Chen, X. Y., Zhang, X. B., Church, J. A., Watson, C. S., King, M. A., Monselesan, D., et al. (2017). The increasing rate of global mean sea-level rise during 1993-2014. *Nature Climate Change*, *7*, 492–495. https://doi.org/10.1038/NCLIMATE3325

Craft, C., Clough, J., Ehman, J., Joye, S., Park, R., Pennings, S., et al. (2009). Forecasting the effects of accelerated sea-level rise on tidal marsh ecosystem services. *Frontiers in Ecology and the Environment*, *7*, 73–78. https://doi.org/10.1890/070219

Dalrymple, R. W., & Choi, K. S. (2007). Morphologic and facies trends through the fluvial-marine transition in tide-dominated depositional systems: A systematic framework for environmental and sequence-stratigraphic interpretation. *Earth-Science Reviews*, *81*, 135–174. https://doi.org/10.1016/j.earscirev.2006.10.002

Dam, G., van der Wegen, M., Labeur, R. J., & Roelvink, D. (2016). Modeling centuries of estuarine morphodynamics in the Western Scheldt Estuary. *Geophysical Research Letters*, *43*, 3839–3847. https://doi.org/10.1002/2015gl066725

Deltares. (2011). User manual Delft3D-flow: Simulation of multi-dimensional hydrodynamic flows and transport phenomena, including sediments, Version 3.15, Deltares.

de Swart, H. E., & Zimmerman, J. T. F. (2009). Morphodynamics of tidal inlet systems. *Annual Review of Fluid Mechanics*, *41*, 203–229. https://doi.org/10.1146/annurev.fluid.010908.165159

Dissanayake, D. M. P. K., Ranasinghe, R., & Roelvink, J. A. (2012). The morphological response of large tidal inlet/basin systems to relative sea level rise. *Climate Change*, *113*(2), 253–276. https://doi.org/10.1007/s10584-012-0402-z

Donatelli, C., Ganju, N. K., Zhang, X., Fagherazzi, S., & Leonardi, N. (2018). Saltmarsh loss affects tides and the sediment budget in shallow bays. *Journal of Geophysical Research: Earth Surface*, *123*, 2647–2662. https://doi.org/10.1029/2018jf004617

Doody, J. P. (2004). Coastal squeeze–a historical perspective. *Journal of Coastal Conservation*, *10*, 129–138. https://doi.org/10.1652/1400-0350(2004)010[0129:csahp]2.0.co;2

Dronkers, J. (1986). Tidal asymmetry and estuarine morphology. *Netherlands Journal of Sea Research*, *20*(2/3), 117–131.

Du, J. B., Shen, J., Zhang, Y. L. J., Ye, F., Liu, Z., Wang, Z. G., et al. (2018). Tidal responses to sea-level rise in different types of estuaries: The importance of length, bathymetry and geometry. *Geophysical Research Letters*, *45*, 227–235. https://doi.org/10.1002/2017gl075963

Edmonds, D. A., & Slingerland, R. L. (2010). Significant effect of sediment cohesion on delta morphology. *Nature Geoscience*, *3*, 105–109. https://doi.org/10.1038/NGEO730

Elmilady, H., van der Wegen, M., Roelvink, D., & Jaffe, B. E. (2019). Intertidal area disappears under sea level rise: 250 years of morphodynamic modeling in San Pablo Bay, California. *Journal of Geophysical Research: Earth Surface*, *124*, 38–59. https://doi.org/10.1029/2018jf004857

Elmilady, H., van der Wegen, M., Roelvink, D., & van der Spek, A. (2022). Modeling the morphodynamic response of estuarine intertidal shoals to sea-level rise. *Journal of Geophysical Research: Earth Surface*, *127*, e2021JF006152. https://doi.org/10.1029/2021jf006152

Engelund, F., & Hansen, E. (1967). *A monograph on sediment transport in alluvial streams*. Teknisk-Forlag.

Ensing, E., de Swart, H. E., & Schuttelaars, H. M. (2015). Sensitivity of tidal motion in well -mixed estuaries to cross-sectional shape, deepening, and sea level rise. *Ocean Dynamics*, *65*(7), 933–950.

Fagherazzi, S., Anisfeld, S. C., Blum, L. K., Long, E. V., Feagin, R. A., Fernandes, A., et al. (2019). Sea level rise and the dynamics of the marsh-upland boundary. *Frontiers in Environmental Science*. https://doi.org/10.3389/fenvs.2019.00025

Fagherazzi, S., Kirwan, M. L., Mudd, S. M., Guntenspergen, G. R., Temmerman, S., D'Alpaos, A., et al. (2012). Numerical models of salt marsh evolution: Ecological, geomorphic, and climatic factors. *Reviews of Geophysics*, *50*, RG1002. https://doi.org/10.1029/2011RG000359

Friedrichs, C. T. (2011). Tidal flat morphodynamics: A synthesis. In B. W. Flemming & J. D. Hansom (Eds.), *Treatise on estuarine and coastal science*, *Estuarine and coastal geology and geomorphology* (Vol. 3, pp. 137–170). Elsevier.

Friedrichs, C. T., & Aubrey, D. G. (1988). Non-linear tidal distortion in shallow well-mixed estuaries: A synthesis. Estuarine. *Coastal and Shelf Science*, *27*, 521–545. https://doi.org/10.1016/0272-7714(88)90082-0

Friedrichs, C. T., Aubrey, D. G., & Speer, P. E. (1990). Impacts of relative sea-level rise on evolution of shallow estuaries. In R. T. Cheng (Ed.), *Residual currents and long-term transport*, *Coastal and estuarine studies* (Vol. 38, pp. 105–120). Springer-Verlag.

Ganju, N. K., Defne, Z., Kirwan, M. L., Fagherazzi, S., D'Alpaos, A., & Carniello, L. (2017). Spatially integrative metrics reveal hidden vulnerability of microtidal salt marshes. *Nature Communications*, *8*, 14156. https://doi.org/10.1038/ncomms14156

Geleynse, N., Storms, J. E. A., Walstra, D.-J. R., Albert Jagers, H. R., Wang, Z. B., & Stive, M. J. F. (2011). Controls on River delta formation: Insights from numerical modeling. *Earth and Planetary Science Letters*, *302*, 217–226. https://doi.org/10.1016/j.epsl.2010.12.013

Geyer, W. R., Woodruff, J. D., & Traykovski, P. (2001). Sediment transport and trapping in the Hudson River estuary. *Estuaries*, *24*(5), 670–679.

Gourgue, O., van Belzen, J., Schwarz, C., Vandenbruwaene, W., Vanlede, J., Belliard, J.-P., et al. (2021). Biogeomorphic modeling to assess resilience of tidal marsh restoration to sea level rise and sediment supply. *Earth surface processes and landforms*. https://doi.org/10.5194/esurf-2021-66

Grasso, F., Bismuth, E., & Verney, R. (2021). Unraveling the impacts of meteorological and anthropogenic changes on sediment fluxes along an estuary-sea continuum. *Scientific Reports*, *11*(1), 1–11.

Gu, J. L., Luo, M., Zhang, X. J., Christakos, G., Agusti, S., Duarte, C. M., & Wu, J. P. (2018). Losses of salt marsh in China: Trends, threats and management. *Estuarine, Coastal and Shelf Science*, *214*, 98–109. https://doi.org/10.1016/j.ecss.2018.09.015

Guo, L. C., van der Wegen, M., Roelvink, D., & He, Q. (2014). The role of river flow and tidal asymmetry on 1D estuarine morphodynamics. *Journal of Geophysical Research: Earth Surface*, *119*, 2315–2334. https://doi.org/10.1002/2014jf003110

Guo, L. C., Xie, W. M., Xu, F., Wang, X. Y., Zhu, C. Y., Meng, Y., et al. (2021). A historical review of sediment export-import shift in the North Branch of Changjiang Estuary. *Earth Surface Processes and Landforms*, *47*, 5–16. https://doi.org/10.1002/esp.5084

Hall, G. F., Hill, D. F., Horton, B. P., Engelhart, S. E., & Peltier, W. R. (2013). High-resolution study of tides in Delaware Bay: Past conditions and future scenarios. *Geophysical Research Letters*, *40*, 338–342. https://doi.org/10.1029/2012gl054675

Hibma, A., de Vriend, H. J., & Stive, M. J. F. (2003). Numerical modeling of shoal pattern formation in well-mixed elongated estuaries. *Estuarine, Coastal and Shelf Science*, *57*, 981–991. https://doi.org/10.1016/s0272-7714(03)00004-0

Hoitink, A. J. F., Nittrouer, J. A., Passalacqua, P., Shaw, J. B., Langendoen, E. J., Huismans, Y., & van Maren, D. S. (2020). Resilience of river deltas in the Anthropocene. *Journal of Geophysical Research: Earth Surface*, *125*, e2019JF005201. https://doi.org/10.1029/2019JF005201

Holleman, R. C., & Stacey, M. T. (2014). Coupling of sea level rise, tidal amplification and inundation. *Journal of Physical Oceanography*, *44*, 1439–1455. https://doi.org/10.1175/jpo-d-13-0214.1

IPCC. (2021). Summary for policymakers. In P., Zhai, A., Pirani, S. L., Connors, C., Péan, S., Berger, N., Caud, et al. (Eds.), *Climate change 2021: The physical science basis. Contribution of working group I to the sixth assessment report of the intergovernmental panel on climate change Masson-Delmotte, V*. Cambridge University Press. In Press.

Jay, D. A. (1991). Green's law revisited: Tidal long-wave propagation in channels with strong topography. *Journal of Geophysical Research*, *96*(C11), 20585–20598.

Kirby, R. (2000). Practical implications of tidal flat shape. *Continental Shelf Research*, *20*, 1061–1077. https://doi.org/10.1016/s0278-4343(00)00012-1

Kirwan, M. L., & Megonigal, J. P. (2013). Tidal wetland stability in the face of human impacts and sea-level rise. *Nature*, *504*, 53–60. https://doi.org/10.1038/nature12856

Kirwan, M. L., Temmerman, S., Skeehan, E. E., Guntenspergen, G. R., & Fagherazzi, S. (2016). Overestimation of marsh vulnerability to sea level rise. *Nature Climate Change*, *6*, 253–260. https://doi.org/10.1038/nclimate2909

Le Hir, P., Roberts, W., Cazaillet, O., Christie, M., Bassoullet, P., & Bacher, C. (2000). Characterization of intertidal flat hydrodynamics. *Continental Shelf Research*, *20*(12–13), 1433–1459. https://doi.org/10.1016/s0278-4343(00)00031-5

Lee, S. B., Li, M., & Zhan, F. (2017). Impact of sea level rise on tidal range in Chesapeake and Delaware Bay. *Journal of Geophysical Research: Oceans*, *122*, 3917–3938. https://doi.org/10.1002/2016jc012597

Lesser, G. R., Roelvink, J. A., Van Kester, J. A. T. M., & Stelling, G. S. (2004). Development and validation of a three-dimensional morphological model. *Coastal Engineering*, *51*, 883–915. https://doi.org/10.1016/j.coastaleng.2004.07.014

Leuven, J. R. F. W., Pierik, H. J., van der Vegt, M., Bouma, T. J., & Kleinhans, M. G. (2019). Sea-level-rise-induced threats depend on the size of tide-influenced estuaries worldwide. *Nature Climate Change*, *9*, 986–992. https://doi.org/10.1038/s41558-019-0606-4

Li, X., Zhang, X., Qiu, C. Y., Duan, Y. Q., Liu, S. A., Chen, D., et al. (2020). Rapid loss of tidal flats in the Yangtze River delta since 1974. *International Journal of Environmental Research and Public Health*, *17*, 1636. https://doi.org/10.3390/ijerph17051636

Lovelock, C. E., Cahoon, D. R., Friess, D. A., Guntenspergen, G. R., Krauss, K. W., Reef, R., et al. (2015). The vulnerability of Indo-Pacific mangrove forests to sea-level rise. *Nature*, *526*, 559–563. https://doi.org/10.1038/nature15538

Luisetti, T., Turner, R. K., Jickells, T., Andrews, J., Elliott, M., Schaafsma, M., et al. (2014). Coastal zone ecosystem services: From science to values and decision making; a case study. *Science of the Total Environment*, *493*, 682–693. https://doi.org/10.1016/j.scitotenv.2014.05.099

Ma, T. T., Li, X. W., Bai, J. H., & Cui, B. S. (2019). Impacts of coastal reclamation on natural wetlands in larger river deltas in China. *Chinese Geographical Science*, *29*, 640–651. https://doi.org/10.1007/s11769-019-1049-8

Mariotti, G., & Canestrelli, A. (2017). Long-term morphodynamics of muddy backbarrier basins: Fill in or empty out? *Water Resources Research*, *53*(8), 7209–7054.

Mazik, K., Musk, W., Dawes, O., Solyanko, K., Brown, S., Mander, L., & Elliott, M. (2010). Managed realignment as compensation for the loss of intertidal mudflat: A short term solution to a long term problem? *Estuarine, Coastal and Shelf Science*, *90*, 11–22. https://doi.org/10.1016/j.ecss.2010.07.009

Murray, A. B., Knaapen, M. A. F., Tal, M., & Kirwan, M. L. (2008). Biomorphodynmics: Physical-biological feedbacks that shape landscapes. *Water Resources Research*, *44*, W11301. https://doi.org/10.1029/2007WR006410

Murray, N. J., Phinn, S. R., DeWitt, M., Ferrari, R., Johnston, R., Lyons, M. B., et al. (2019). The global distribution and trajectory of tidal flats. *Nature*, *565*, 222–225. https://doi.org/10.1038/s41586-018-0805-8

Nienhuis, J. H., Ashton, A. D., Edmonds, D. A., Hoitink, A. J. F., Kettner, A. J., Rowland, J. C., & Tornqvist, T. E. (2020). Global-scale human impact on delta morphology has led to net land area gain. *Nature*, *577*, 514–518. https://doi.org/10.1038/s41586-019-1905-9

Obodoefuna, D. C., Fan, D. D., Guo, X. J., & Li, B. (2020). Highly accelerated siltation of abandoned distributary channel in the Yangtze Delta under everchanging social-ecological dynamics. *Marine Geology*, *429*, 106331. https://doi.org/10.1016/j.margeo.2020.106331

Olabarrieta, M., Geyer, W. R., Coco, G., Friedrichs, C. T., & Cao, Z. (2018). Effects of density-driven flows on the long-term morphodynamic evolution of funnel-shaped estuaries. *Journal of Geophysical Research: Earth Surface*, *123*(11), 2901–2924.

Orton, P. M., Talke, S., Jay, D. A., Yin, L., Blumberg, A. F., Georgas, N., et al. (2015). Channel shallowing as mitigation of coastal flooding. *Journal of Marine Science and Engineering*, *3*, 654–673. https://doi.org/10.3390/jmse3030654

Pelling, H. E., Green, J. A. M., & Ward, S. L. (2013). Modelling tides and sea-level rise: To flood or not to flood. *Ocean Modelling*, *63*, 21–29. https://doi.org/10.1016/j.ocemod.2012.12.004

Pethick, J. S. (1994). Estuaries and wetlands: Function and form. In *Wetland management* (pp. 75–87). Thomas Telford.

Reed, D., van Wesenbeeck, B., Herman, P. M. J., & Meselhe, E. (2018). Tidal flat-wetland systems as flood defenses: Understanding biogeomorphic controls. *Estuarine, Coastal and Shelf Science*, *213*, 269–282. https://doi.org/10.1016/j.ecss.2018.08.017

Ridderinkhof, W., de Swart, H. E., van der Vegt, M., Alebregtse, N. C., & Hoekstra, P. (2014). Geometry of tidal inlet systems: A key factor for the net sediment transport in tidal inlets. *Journal of Geophysical Research: Oceans*, *119*(10), 6988–7006. https://doi.org/10.1002/2014jc010226

Rodriguez, J. F., Saco, P. M., Sandi, S., Saintilan, N., & Riccardi, G. (2017). Potential increase in coastal wetland vulnerability to sea-level rise suggested by considering hydrodynamic attenuation effects. *Nature Communications*, *8*, 16094. https://doi.org/10.1038/ncomms16094

Roelvink, J. A., & Reniers, A. J. H. M. (2011). *A guide to coastal morphology modeling*. In *Advances in Coastal and Ocean Engineering* (Vol. 12). World Sci. Co.

Ross, A. C., Najjar, R. G., Li, M., Lee, S. B., Zhan, F., & Liu, W. (2017). Fingerprints of sea level rise on changing tides in the Chesapeake and Delaware Bays. *Journal of Geophysical Research: Oceans*, *122*, 8102–8125. https://doi.org/10.1002/2017jc012887

Schuerch, M., Spencer, T., Temmerman, S., Kirwan, M. L., Wolff, C., Lincke, D., et al. (2018). Future response of global coastal wetlands to sea-level rise. *Nature*, *561*, 231–234. https://doi.org/10.1038/s41586-018-0476-5

Sommerfield, C. K., & Wong, K. C. (2011). Mechanisms of sediment flux and turbidity maintenance in the Delaware Estuary. *Journal of Geophysical Research*, *116*, C01005. https://doi.org/10.1029/2010jc006462

Speer, P. E., & Aubrey, D. G. (1985). A study of non-linear tidal propagation in shallow inlet/estuarine systems Part II: Theory. Estuarine. *Coastal and Shelf Science*, *21*, 207–224. https://doi.org/10.1016/0272-7714(85)90097-6

Spencer, T., Schuerch, M., Nicholls, R., Hinkel, J., Lincke, D., Vafeidis, A. T., et al. (2016). Global coastal wetland change under sea-level rise and related stresses: The DIVA wetland change model. *Global and Planetary Change*, *139*, 15–30. https://doi.org/10.1016/j.gloplacha.2015.12.018

Stein, E. D., Dark, S., Longcore, T., Grossinger, R., Hall, N., & Beland, M. (2010). Historical ecology as a tool for assessing landscape change and informing wetland restoration priorities. *Wetlands*, *30*, 589–601. https://doi.org/10.1007/s13157-010-0050-x

Syvitski, J. P. M., Kettner, A., Overeem, I., Hutton, E. W. H., Hannon, M. T., Brakenridge, C. R., et al. (2009). Sinking deltas due to human activities. *Nature Geoscience*, *2*, 681–686. https://doi.org/10.1038/ngeo629

Talke, S. A., & Jay, D. A. (2020). Changing tides: The role of natural and anthropogenic factors. *Annual Review of Marine Science*, *12*, 121–151. https://doi.org/10.1146/annurev-marine-010419-010727

Temmerman, S., Meire, P., Bouma, T. J., Herman, P. M. J., Ysebaert, T., & de Vriend, H. J. (2013). Ecosystem-based coastal defense in the face of global change. *Nature*, *504*, 79–83. https://doi.org/10.1038/nature12859

Thorne, K., MacDonald, G., Guntenspergen, G., Ambrose, R., Buffington, K., Dugger, B., et al. (2018). U.S. Pacific coastal wetland resilience and vulnerability to sea-level rise. *Science Advances*, *4*(2). https://doi.org/10.1126/sciadv.aao3270

Townend, I. H., & Pethick, J. (2002). Estuarine flooding and managed retreat. *Philosophical Transactions of the Royal Society London A*, *360*(1796), 1477–1495.

Townend, I. H., & Whitehead, P. (2003). A preliminary net sediment budget for the Humber Estuary. *Science of the Total Environment*, *314*, 755–767. https://doi.org/10.1016/s0048-9697(03)00082-2

Townend, I. H., Zhou, Z., Guo, L. C., & Coco, G. (2021). A morphological investigation of marine transgression in estuaries. *Earth Surface Processes and Landforms*, *46*, 626–641. https://doi.org/10.1002/esp.5050

Valiela, I., Lloret, J., Bowyer, T., Miner, S., Remsen, D., Elmstrom, E., et al. (2018). Transient coastal landscapes: Rising sea level threatens salt marshes. *Science of the Total Environment*, *640–641*, 1148–1156. https://doi.org/10.1016/j.scitotenv.2018.05.235

van de Lageweg, W. I., & Slangen, A. B. A. (2017). Predicting dynamic coastal delta change in response to sea-level rise. *Journal of Marine Science and Engineering*, *24*, 1–12.

van der Wegen, M. (2013). Numerical modeling of the impact of sea level rise on tidal basin morphodynamics. *Journal of Geophysical Research: Earth Surface*, *118*, 447–460. https://doi.org/10.1002/jgrf.20034

van der Wegen, M., & Roelvink, J. A. (2008). Long-term morphodynamic evolution of a tidal embayment using a two-dimensional, process-based model. *Journal of Geophysical Research*, *113*, C03016. https://doi.org/10.1029/2006JC003983

van Maanen, B., Coco, G., Bryan, K. R., & Friedrichs, C. T. (2013). Modeling the morphodynamic response of tidal embayments to sea-level rise. *Ocean Dynamics*, *63*, 1249–1262. https://doi.org/10.1007/s10236-013-0649-6

Wang, Z. B., Elias, E. P. L., van der Spek, A. J. F., & Lodder, Q. J. (2018). Sediment budget and morphological development of the Dutch Wadden sea: Impact of accelerated sea-level rise and subsidence until 2100. *Netherlands Journal of Geosciences*, *97*, 183–214. https://doi.org/10.1017/njg.2018.8

Xu, K. H., Bentley, S. J., Day, J. W., & Freeman, A. M. (2019). A review of sediment diversion in the Mississippi River Deltaic plain. *Estuarine, Coastal and Shelf Science*, *225*, 106241. https://doi.org/10.1016/j.ecss.2019.05.023

Zedler, J. B. (2004). Compensating for wetland losses in the United States. *Ibis*, *146*(S1), 92–100.

Zhang, X. H., Leonardi, N., Donatelli, C., & Fagherazzi, S. (2020). Divergence of sediment fluxes triggered by sea-level rise will reshape coastal bays. *Geophysical Research Letters*, *47*(13), e2020GL087862. https://doi.org/10.1029/2020GL087862

Zhou, Z., Chen, L. Y., Tao, J. F., Gong, Z., Guo, L. C., van der Wegen, M., et al. (2020). The role of salinity in fluvio-deltaic morphodynamics: A long-term modeling study. *Earth Surface Processes and Landforms*, *45*, 590–604. https://doi.org/10.1002/esp.4757

Zhou, Z., Coco, G., Townend, I., Gong, Z., Wang, Z. B., & Zhang, C. K. (2018). On the stability relations between tidal asymmetry and morphologies of tidal basins and estuaries. *Earth Surface Processes and Landforms*, *43*, 1943–1959. https://doi.org/10.1002/esp.4366